Master Thesis

Ground penetrating radar for road monitoring and damage detection: The Layer-Stripping Algorithm

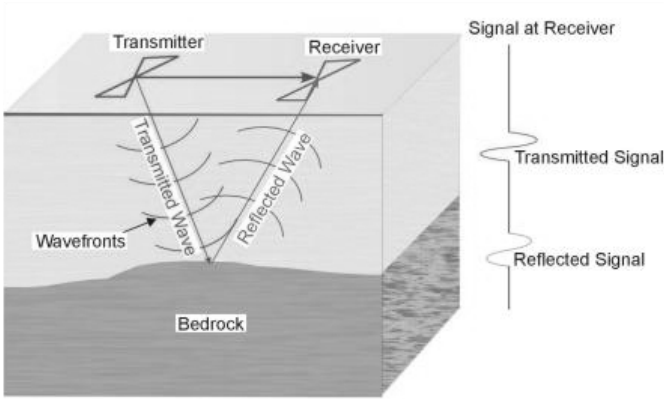

Daniel Viedma Parrilla

GPR for road monitoring and damage detection: The Layer-Stripping Algorithm

Master Thesis by: Daniel Viedma Parrilla (ETSETB)

Supervised by:
Prof. Ing. Andrea Benedetto
Prof. Ing. G. Giunta
Prof. Ing. G. Cincotti

Università degli studi Roma Tre
Dipartamento Ingegneria Elettronica
Dipartamento Ingegneria Civile

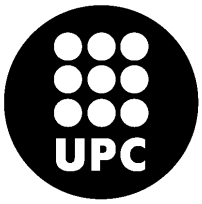

Roma, October 2006

Index

Acknowledgements

First I would like to thank everyone at the Università degli Studi Roma Tre for the warm welcome they did to me. I trully felt as one of them.

Very special thanks to Prof. Andrea Benedetto, who trust me from the very first moment to do the research. He guided me and gave the incredible chance to apply the work done at the Linate Airport (Milano), which is explained at Chapter 6.

Special mention also to 'Spartaco', the laboratory chief at the *Dipartamento Ingegneria Civile*, who always had the time to help you out at the lab. Together with him and Prof. Benedetto we did the Milano expedition.

Chapter 1
Introduction

1.1 Introduction

Programmed policies for pavement management are needed because of the wide structural damage, that implies consequences for the safety and operability of road networks. In fact, during the last decade, road networks suffered from great structural damages, imputable to different reasons, such as the increasing traffic or the lack of means for routine maintenance. A local anomaly on the road surface can affect the safety of driving according to the use of the road, so it is possible to set up different rehabilitations according to the different standards of road. Many damages, coming from the bottom layers and invisible until pavement cracks, depend on the infiltration of water and plastic soil that reduces greatly the bearing capacity of sub-asphalt structural layers and soils. On the basis of an in-depth recent international literature overview, an experimental survey with Ground Penetrating Radar (GPR) was led to calibrate the geophysical parameters and to validate the reliability of an indirect diagnostic method of pavement damages.

The experiments were set on a pavement under where water was injected over a period of several hours: GPR travel time data were used to estimate the dielectric constant and the water content in un-bound aggregate layer, the variations in water content with time and particular areas where effective velocity of infiltration decreases. A new methodology has been finally proposed to extract from the moisture maps observed with GPR the hydraulic permittivity fields in sub-asphalt

structural layers and soils. It is effective to diagnose the presence of clay or plastic soil that compromises the bearing capacity of sub-base and induces damages.

1.2 Motivation of the work

All over the world, in industrialized as well as in developing countries, the networks of roads suffered from significant structural damages because of different reasons, such as the increasing traffic and the lack of means for routine maintenance (i.e. Shahin, 1994, Aultman-Hall et al. 2004, Robinson and Thagesen, 2004). This fact has brought about not negligible consequences as far as driving safety is concerned, since the damage of pavements creates significant risks for drivers (PRIN, 1999; Tighe et al. 2000; Guell et al. 2003).
Therefore several recent initiatives were taken in order to recover the functionality of the road network both in EU as in USA and many industrialized countries.

The traditional approach to the Pavement Management System (PMS) consists of the ability both to determine the current condition of a pavement network and to predict its future performance. The use of Pavement Condition Index (PCI) has received wide acceptance by now and has been formally adopted as standard procedure by many agencies worldwide (Cuvillier and al 1987; Shahin, 1994). Because of PCI, as similar diffused "mechanically based" approaches, was originally developed to describe the structural condition of pavement and road, it totally neglects the effect of damages on driving safety. As it will be later mentioned, new trends have been developing that take into consideration that a pavement damage is not critical by itself but only if it becomes dangerous for driving. For example the damage is dangerous when the rutting is so deep that, in case of rainfall, the water film is so thick that skid drastically decreases. Moreover the same damage can be dangerous on motorway and secure on an urban road because the operating speeds are different. These facts are usually neglected under a traditional PCI approach.

In detail, the current limits of PCI, under a perspective that is wider rather than the original reasons of PCI development, can be summarized as it follows: (i) it gives aggregated information about the pavement condition unless considering the specific damage, (ii) it neglects the causes of the damage, (iii) it can not suggest any rehabilitation action, but only the need of rehabilitation, (iv) it can assume the same value for damaged pavements that apparently are similar but that can be distressed in completely different ways and for completely different causes, (v) it does not predict the evolution of the pavement performance, (vi) it does not consider the impact of damage on driving safety.

Other quantitative indexes have been proposed, such as the International Roughness Index (IRI) or the Skid Number (SN), in order to quantify specific defects of the pavement. They seem to be

more useful to identify the impact on safety and the best rehabilitation action, however they measure the effect and they give no information about the causes.

The damage of roads reveals itself in several ways, for example superficial anomalies are clearly visible. Structural damages that begin from deep layers, such as subgrade or sub-base, become visible only later, when the pavement is completely failed.
These phenomenon are always irreversible and rehabilitations are relevant and expensive.

Structural damage in road pavements is frequently directly connected with the percentage of moisture in the deepest layers of it or in the subgrade soils: water infiltration and clayey soils pumping is one of the most important cause of the decrease of bearing capacity of the unbound layers (Kelley, 1999; Rainwater et al. 2001; Al-Qadi et al. 2004; Zuo et al. 2004, Diefenderfer et al. 2005).

We can define the bearing capacity as the ability to carry a defined number of repetitions of a set of loads. Rational design methods are used in order to understand the stress and strain conditions due to the action of loads and temperature changes. In fact, the entity of strain generates the slow or fast evolution of fatigue and the phenomenon of the accumulation of permanent strains.
To characterize the elastic behaviour of the sub-asphalt unbound layers pavement engineers usually refer to the resilient modulus, that considers only the completely given strain: it is the ratio between the stress applied and the strain returned (i.e. Hicks, 1970; Rahim and George, 2005). Since the status of stress in the aggregate layer varies in relation to the bearing capacity of the sub-grade, if we do not assess it accurately, programmed policy could be inadequate or useless.
Road engineers have tools for local diagnostics. Yet these diagnostic tools are destructive and are characterized by so inadequate time and costs that Administration and Agencies cannot manage the local road network, above all when studies have to be repeated periodically to update the database and when they involve areas of thousands of km.

Nowadays the most used non destructive method to estimate the bearing capacity of a subgrade is the Falling Weight Deflectometer (FWD), through which it is possible to assess the elastic modulus of the subgrade and the aggregate layers, so we can obtain a behavioural scheme of the whole pavement (i.e. Mehta and Roque, 2003). The FWD is a device capable of applying dynamic loads to the pavement surface, similar in magnitude and duration to that of a single heavy moving wheel load.

Moisture has an important role, because if it increases, stiffness decreases so strains increase too.
A widely used method to measure soil water content, bulk electrical conductivity, and deformation of rock is based on Time Domain Reflectometry system (TDR). TDR measurements are non destructive but offer excellent accuracy and precision: it is the analysis of a conductor (wire, cable, or fiber optic) by sending a pulsed signal into the conductor, and then examining the reflection of

that pulse (Weiler et al. 1998). FWD and TDR methods for wide roads inspection are not generally efficient in terms of time and cost.

Moreover, as moisture in sub-grade is not spatially homogeneous, these methods are limited, because they provide only local measurements and they cannot be used in wide areas. On the contrary, GPR systems are suitable to the aim, in fact they are non destructive and quick if used large scale.

To obtain significant measures non-local studies are needed, because moisture conditions change as to the effective survey moment: a GPR allows quick measures and obtains data that reflect the real physical conditions of the subgrade soil.

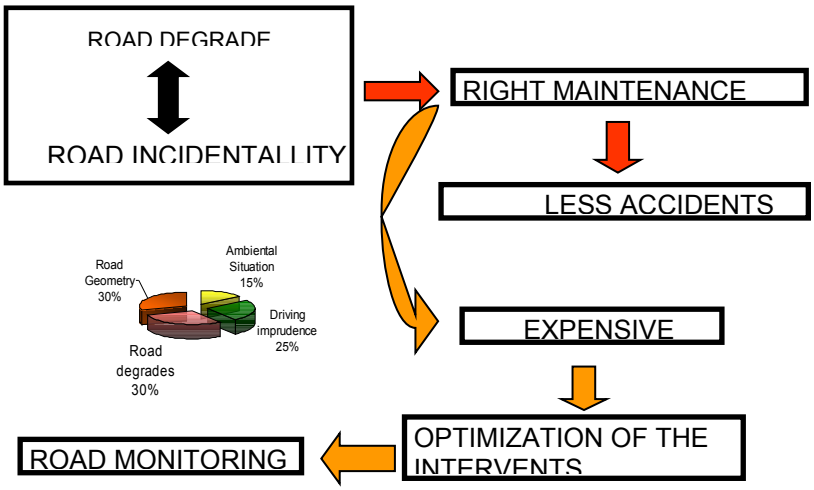

Fig. 1.1.

This work aims to provide a tool that can opportunely direct means to best plan maintenance and consequently contributing to decrease the consequences of structural damage on driving safety.

The next sections describe the background, the theoretical and methodological approach, the experiments, the data collection, processing and interpretation techniques.

1.3 Objective of the Thesis

Without the right signal processing technique, the GPR tool would became useless. . With an appropiate algorithm we can exploit and use all the amout of data that the GPR provide us.

Hence, the objective of the thesis is elaborate a signal processing algorithm in *Matlab*. This algorithm must be able to extract a synthetic map of the ground. This means that the algorithm has

to calculate **layer thickness** and **permitittivity** of each layer that forms the pavement structure and draw the map colouring the different permitittivity areas. The algorithm should be fully configurable by the user depending on the particular zone to scan and, last but not least, it must be user-friendly.

At the "Unversità Roma Tre" they would have a previous algorithm I would have to study and try to enhance.

The 'Università Roma Tre' current algorithm

The current signal processing technique used for pavement damages detection and classification using GPR is the one described in [1]. It only uses the time-delay information of the reflected echoes to detect and classify possible damages.

The GPR device moves longitudinaly through the road emiting and reciving a radar signal. Each interface between two different layers produces a reflected signal. Looking the delay of that signal you can predict the thickness of that layer, as you have the velocity and the time used to go through the layer. To detect a possible anomaly in a specific interface the algorithm compares the normal delay of that interface (that is an average of delays induced by the interfarce along the road) with the delay of each radar sweep in the same interface. If the difference between these two delays is greater than a fixed threshold it means that there is an anomaly, given that an increment (or decrement) of the time-delay can be traduced in an increment or decrement of the layer thickness.

That anomaly can not be caused only by an increment or decrement of the layer thickness, but also by the presence of a point-located singularity inside a homogeneous layer (i.e., void or water).

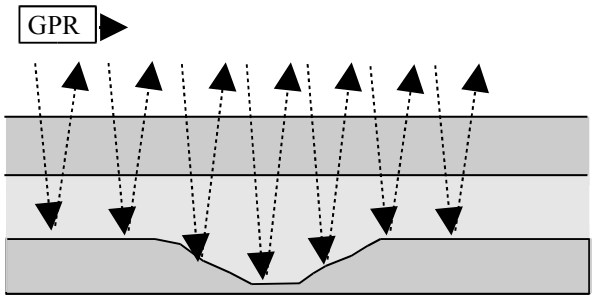

Fig. 1.2. There is an anomaly between the 2nd and the 3rd layer. The 4th sweep detects it, as the time delay is different than the rest of the sweeps of that interface

Problems and drawbacks

In the explication above we are suposing that the velocity of propagation of the radar signal is fixed and it doesnt change along the scan. It is, that the permettivity doesnt change along the layer. But what if it wasnt truth? If the permettivty changes along the layer then the velocity of

propagation also changes. If velocity changes, then the time-delay so does, given us the wrong impression that there is an anomaly in the interface.

A tipical situation could be an increase of the water content in a part of the layer, that is an increase of the permettivity of the medium, wich means a reduction of the velocitiy of propagation and and increment of the time-delay. Moreover, that problem can not be detected easely, as the radar can only detect changes between layers with a significant difference in terms of permettivity.

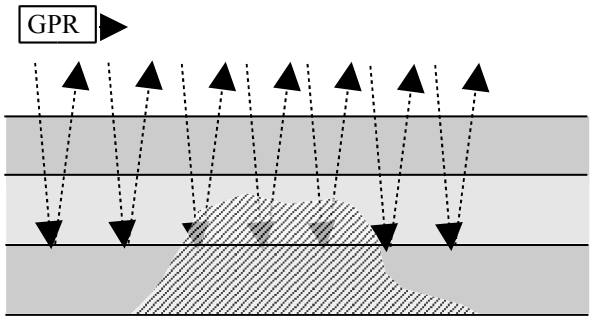

Fig. 1. 3. A stain of water is growing from the base of the road layering, increasing the permettivity of the 2nd and the 3rd layer. The interface shows no damage, but the time delay on the 4th sweep makes us think the contrary, as it is greater than the rest. Note that $v = c/\sqrt{\varepsilon}$

It is difficult to discern in terms of echo-delay between when we have a real layer deformation than when we have a change of permettivity in the medium.

In that case of ambiguity only a verification in situ with extractions of some sample cores would make the decision reliable.

The goal is achieve a signal processing technique that make that decision as reliable as posible with the maximum economy of resources. That is, redoucing the ambiguous situations detected and contsecuently, the samples cores needed.

It would be useful to have a signal processing algorithm that can not only estimate the layer thickness but also the permittivity (in average) of the layer. That tool would be such a ”decision assistant” for the professional in charge. Having a complete pavement profiling, a proffessional could probably reject some impossible cases. Moreover, the algorithm would be able to assess some kind of probability of real damage detected, in case of ambiguity or anomality along de pavement scan.

The presence of a professional in the field is always requiered.

Chapter 2
GPR theoretical bases

2.1. Introduction: Mawell's equations

GPR is a diagnostic non destructive technology based on the transmitting/receiving of a high frequency electromagnetic signal. The analysis of phase, frequency and amplitude differences between the transmitted and the received signal gives information about the electromagnetic properties of the media through which the signal is transmitted, reflected or scattered

Applications of GPR include locating buried voids/cavities, underground storage tanks, sewers, buried foundations, ancient landfills. It can also be used to characterize bedrock, ice, the internal structure of floors/walls, water damage in concrete, and the internal steelwork in concrete.

GPR uses transmitting and receiving antenna. The transmitting antenna radiates short pulses of the high-frequency (usually polarized) radio waves into the ground. When the wave hits a buried object or a boundary with different dielectric constants, the receiving antenna records variations in the reflected return signal. The principles involved are similar to reflection seismology, except that electromagnetic energy is used instead of acoustic energy, and reflections appear at boundaries with different dielectric constants instead of acoustic impedances.

The depth range of GPR is limited by the electrical conductivity of the ground, and the transmitting frequency. Higher frequencies do not penetrate as far as lower frequencies, but give better resolution. Optimal depth penetration is achieved in dry sandy soils or massive dry materials such as granite, limestone, and concrete where the depth of penetration is up to 15 m. In moist and/

or clay laden soils and soils with high electrical conductivity, penetration is sometimes only a few centimetres.

Ground-penetrating radar antennae are generally in contact with the ground for the strongest signal strength; however, GPR horn antennae can be used 0.3 to 0.6 m above the ground.

The behavior of both the electric and magnetic fields and its sources are defined by the Maxwell's Equations. Developing this equations and adding the Continuity Equations (for zones where there are surface distribution of charge) we can determine how the wave behave and its propagation through a medium.

$$\nabla \times H = J + \frac{\partial D}{\partial t} \qquad (1) \qquad \text{Ampère's law}$$

$$\nabla \times E = -\frac{\partial B}{\partial t} \qquad (2) \qquad \text{Faraday's law}$$

$$\nabla \times D = \rho \qquad (3) \qquad \text{Gauss's law}$$

$$\nabla \times B = 0 \qquad (4) \qquad \text{Gauss's law}$$

Where E is the electric field (V/m), H is the magnetic field (A/m), D is the electric displacement field (C/m2), B is the the magnetic induction (W/m2), ρ free electric charge density (C/m3), J is the free current density (A/m2)
In non-dispersive, isotropic media reduce to.

$$\nabla \cdot \varepsilon E = \rho \qquad (5)$$

$$\nabla \cdot \mu H = 0 \qquad (6)$$

$$\nabla \times E = -\mu \frac{\partial H}{\partial t} \qquad (7)$$

$$\nabla \times H = J + \varepsilon \frac{\partial E}{\partial t} \qquad (8)$$

Where ε is the electrical permittivity or dielectric constant of the material, and μ is the magnetic permeability of the material.

These equations have a simple solution in terms of travelling sinusoidal plane waves, with the electric and magnetic field directions orthogonal to one another and the direction of travel, and with the two fields in phase.

Taking as a possible solution to these equations:

$$E = E_0 e^{-jkz} \qquad (9)$$

Where k is the propagation constant:

$$k = \omega \sqrt{\mu \varepsilon (1 - j \tan\delta)} \qquad (10)$$

$$\tan\delta = \frac{\frac{\sigma}{\varepsilon_0} + \omega \varepsilon_r''}{\omega \varepsilon_r'} \qquad (11)$$

$\varepsilon_0 = 8.854 \cdot 10^{-12}$ Permittivity of free space (F/m)

$\varepsilon_r' = \frac{\varepsilon'}{E}$ (12) Real part of the relative permittivity.

$\varepsilon_r'' = \frac{\varepsilon''}{\varepsilon_0}$ (13) Imaginary part of the relative permittivity.

So finally we get the 'Electromagnetic wave equation for the electric field':

$$\frac{\partial^2 E}{\partial z^2} = -\omega^2 \mu \varepsilon E \qquad (14)$$

There are two parameters in the expresión above of particular interest in our study: Attenuation and dielectric constant. We will see why…

Going on with the 'Electromagnetic wave equation', it is possible to transform the solution above given to demonstrate the distortion suffered by the wave through a medium. In particular, given that:

$$\alpha = \omega \sqrt{\frac{\mu \varepsilon}{2}\left(\sqrt{1+\tan^2\delta} - 1\right)} \quad (15)$$

$$\beta = \omega \sqrt{\frac{\mu \varepsilon}{2}\left(\sqrt{1+\tan^2\delta} + 1\right)} \quad (16)$$

Since we have α in neper/m and β in rad/m, it is possible to rewrite the solution as follows:

$$E = E_0 e^{-\alpha z} e^{-j\beta z} \quad (17)$$

The term $e^{-j\beta z}$ is attetuation and distortion factor of the signal amplitude. As it is evident, depends on the medium electric properties.

The wave propagation speed can be expressed as a function of the medium electric properties too. Here it is:

$$\frac{v}{c} = \frac{\sqrt{2\varepsilon_0}}{\sqrt{\varepsilon' - \frac{\sigma''}{\omega}}}\left[\sqrt{1+\left(\frac{\varepsilon'' + \frac{\sigma}{\omega}}{\varepsilon' - \frac{\sigma}{\omega}}\right)^2} + 1\right]^{-0.5} \quad (18)$$

Where:

$$c = \text{wave velocity in free space} = 3 \cdot 10^5 \text{ km/s} = \frac{1}{\sqrt{\varepsilon_0 \mu_0}}$$

Considering that $\omega >> \sigma'$, $\omega >> \sigma''$ and that $\varepsilon'' >> \varepsilon'$, it is posible to aproximate the precedent expression into this one:

$$v = \frac{c}{\sqrt{\frac{\varepsilon'}{\varepsilon_0}}} = \frac{c}{\sqrt{\varepsilon_r'}} \quad (19)$$

2.2. Permittivity, water content and velocity

Why is it so important the attenuation and the dielectric constant for our study?

The materials used in the road construction area have certain electric, phsysic and mechanic properties. For our objectives, the most important parameters are the DIELECTRIC CONSTANT (permittivity) and the ATTENUATION.

We call **dielectric** all substances that have the propertie of reducing the potential difference between the plates of a capacitor. This way, the physic definition of dielectric is given by the concept of Volt:

$$\varepsilon = \frac{V_0}{V_\varepsilon} \qquad (20)$$

Relative dielectric permittivity (RDP), also called the dielectric constant, is a measure of the ability of a material to store a charge from an applied electromagnetic field and then transmit that energy. It is usually determined empirically from measurements in the field but can be directly measured in the laboratory. In general, the greater the RDP of a material, the slower radar energy will move through it. Relative dielectric permittivity is a measurement of how well radar energy will be transmitted to depth. It therefore not only measures velocity of propagating radar energy, but also its strength.

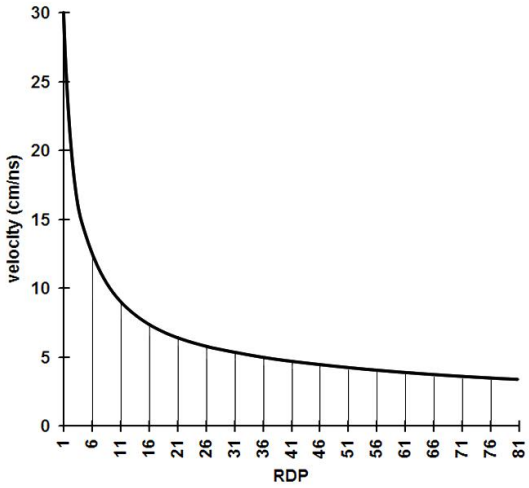

Fig. 2.1. Relative dielectric permittivity is inversely related to radar travel velocity.

RDP is the ratio of a material's electrical permittivity to the electrical permittivity in a vacuum (that is defined as one). Relative dielectric permittivities of materials vary somewhat with their composition, but the greatest factor affecting RDP is moisture content and its distribution. Bulk

density, porosity, physical structure and temperature will all affect the moisture content, but by themselves are not the controlling factor, as they all affect moisture in some fashion.

Many erroneously view a measurement of RDP as a definitive measurement of how effective a material will be in transmitting energy to depth in the ground. In reality it is mostly a measurement of how effectively an electromagnetic wave can move, and therefore is more a measure of velocity rather than overall ability to transmit energy. For instance, the RDP of fresh water is very high (about 80), but radar energy can easily be transmitted through it without being attenuated (especially when frozen).

A bed of peat, which is composed almost wholly of organic material and fresh water, also has a high RDP but will also allow radar transmission to great depths, but at much slower speeds than in saturated sand or other materials. The relative dielectric permittivity of air, which exhibits only negligible electromagnetic polarization, is approximately 1.0003, and is usually rounded to one.

The RDP of many naturally occurring materials in the ground, in a totally dry state, varies little, usually between about 3 and 5. But if just a small amount of water is added to the material (which is almost always the case in natural conditions, even in the driest of deserts) the RDP will increase. In order to generate a significant reflection in a profile, the change in RDP between two bounding materials must occur over a short distance. When the RDP changes gradually with depth only small differences in reflectivity will occur every few centimeters in the ground and weak or no reflections at all will be generated.

It is always important to know the RDP (or velocity) of the material at each site being studied, as it will be used to convert radar travel times to depth.

Typical relative dielectric permittivities (RDPs) of common geological materials. Modified from Davis and Annan (1989) and Geophysical Survey Systems, Inc. (1987).

Material	**RDP**
Air	1
Dry sand	3-5
Dry silt	3-30
Ice	3-4
Asphalt	3-5
Volcanic ash/pumice	4-7
Limestone	4-8
Granite	4-6
Permafrost	4-5
Coal	4-5
Shale	5-15

Clay	5-40
Concrete	6
Saturated silt	10-40
Dry sandy coastal land	10
Average organic-rich surface soil	12
Marsh or forested land	12
Organic rich agricultural land	15
Saturated sand	20-30
Fresh water	80
Sea water	81-88

Fig. 2.2.

As we see at the table, water is the greater value, while the materials used in the road field have values between 2 and 6.

The value of the dielectric constant of a composed material, lets say a mix of minerals, air and water, is given basicly by:

1. The dielectric constants of the diferent substances that compose the material
2. The volumetric fractions
3. Geometric characteristics
4. Electrochemical interactions

It is interesting to note the variation of the dielectric and mechanic properties of the materials examinated depending on the water content, for the most usual values of frequencies used on the GPR for road monitoring.

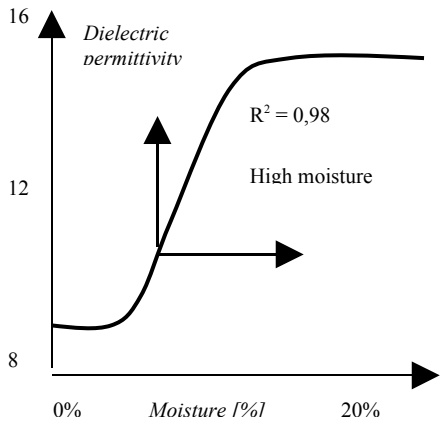

Fig. 2.3. Correlation between Dielectric Constant - Water Content

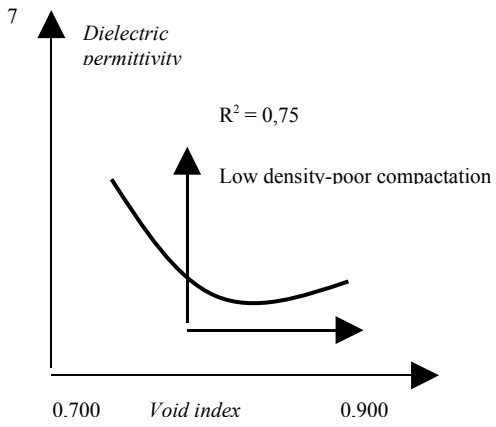

Fig. 2.4. Dielectric Constant VS Void Index

At the figure is shown the dielectric constant variation versus the water content. The increase of the relative dielectric constant is due to the great polarization properties of the water. However, it depends a lot on the different materials and the volumetric fractions that form it.

On the other hand, this increase of the water content can saturate the media and consequently, transform part of the water content already absorbed into "free water", breaking the molecular links and weakening the whole structure.

For the sake of completeness, down below are shown the values for the dielectric constant at ambient temperature and 1GHz frequency for most common materials used at road pavement.

DIELECTRIC CONSTANTS FOR MOST USED MATERIALS AT PAVEMENT				
Bitumen	**Limestone**	**Agglomerate. hot mixed**	**Air**	**Water**
agglomerate.	3 - 9	4 - 6	1	81
2 - 6				

Fig 2.5. Dielectric constant at ambient temperature and 1GHz frequency for most common materials used at road pavement

2.3. Attenuation

Attenuation, instead, express the diminution of the signal intensity traveling through a material. It could be considered a complex function of the electrical conductivity (another physic property of the materials) and is given in dB/m. In general, it could be said that the depth of the maximum scan obtainable in a certain material is limited by its value of the attenuation.

High values are found at materials characterized by high values of electrical conductivity, like limestone, clay, metals and saline water. On the other hand, low values typical for crystalline rocks, gravel, sand and unmineralized water. Though with different intensity, the water presence is responsible of increasing ε and attenuation values.

Materials characterized by high values of attenuation limit remarkably the depth of the scan: in clay plastic is reduced to a few centimeters and in metals is almost zero.
This discourse highlight the close correlation between some fundamental parameters of the compost agglomerate and the GPR response. In particular, and with the pavement monitoring as our goal, some important features of the medium that we can study using GRP techniques are:

a) Medium classification: The electrical properties of the materials depend on (among other reasons) the kind of material used. Therefore, it is possible to characterize the media that we are studying.

b) Water content: The electrical properties of the materials are remarkably influenced by the water content. Therefore, it is possible to specify the moisture of the aggregate.

c) Medium conditions: soil compaction, buried object detection, etc.

As we see, the dielectric constant is crucial for:

- Media classification
- Water content
- Variation of mechanic properties of the media (compaction, etc.)

2.4. Reflection and refraction

When the electromagnetic energy reach an interface between different media it is produced reflection and refraction phenomenons.

Snell's law (also known as Descartes' Law or the law of refraction), is a formula used to describe the relationship between the angles of incidence and refraction, passing through a boundary between two different isotropic media, such as air and glass. The law says that the ratio of the sines of the angles of incidence and of refraction is a constant that depends on the media.

The percentage of energy reflexed depends on the contrast between the electromagnetic parameters of the different materials of the media. This percentage defines the transmission and reflection coefficients.

The impedance of an electromagnetic field is the quotient between the magnetic and the electric field. It can be defined an impedance for the incident electromagnetic field, N1, that will match with the impedance of the reflected electromagnetic field, and an impedance for the refracted electromagnetic field, N2, it is, transmitted:

$$\eta_1 = \left\{ \frac{\vec{E}_i}{\vec{H}_i} = \sqrt{\frac{\mu_o \mu_r}{\varepsilon_0 \varepsilon_r}} \right\} = \left\{ \frac{\vec{E}_r}{\vec{H}_r} = \sqrt{\frac{\mu_o \mu_r}{\varepsilon_0 \varepsilon_r}} \right\} \quad (21)$$

$$\eta_2 = \left\{ \frac{\vec{E}_t}{\vec{H}_t} = \sqrt{\frac{\mu_o \mu_{r2}}{\varepsilon_0 \varepsilon_{r2}}} \right\} \quad (22)$$

Taking this expressions, it can be possible to obtain the reflection and the refraction energy coefficients of Fresnel

$$R_{1\to 2} = \frac{\vec{E}_r}{\vec{E}_i} = \frac{\eta_2 \cos(at) - \eta_1 \cos(ai)}{\eta_1 \cos(ai) + \eta_1 \cos(at)} \quad (23)$$

$$T_{1\to 2} = \frac{\vec{E}_t}{\vec{E}_i} = \frac{2\eta_2 \cos(at)}{\eta_1 \cos(ai) + \eta_2 \cos(at)} \quad (24)$$

For the GPR studies it can be possible to simplify these expressions, since the the reflection angle is very small, rounding to zero the incidence and reflection angles. It is, perpendicular incidence.

$$R = \frac{\eta_1 - \eta_2}{\eta_1 + \eta_2} = \frac{\sqrt{\varepsilon_{r_1}} - \sqrt{\varepsilon_{r_2}}}{\sqrt{\varepsilon_{r_1}} + \sqrt{\varepsilon_{r_2}}} \quad (25)$$

$$T = \frac{2\eta_2}{\eta_1 + \eta_2} = \frac{2\sqrt{\varepsilon_{r_2}}}{\sqrt{\varepsilon_{r_1}} + \sqrt{\varepsilon_{r_2}}} \quad (26)$$

We can deduce from these expressions that the greater is difference between the media (in terms of electromagnetic parameters), the greater is the reflection coefficient, it is, more percentage of the incident energy will be reflected instead of transmitted.

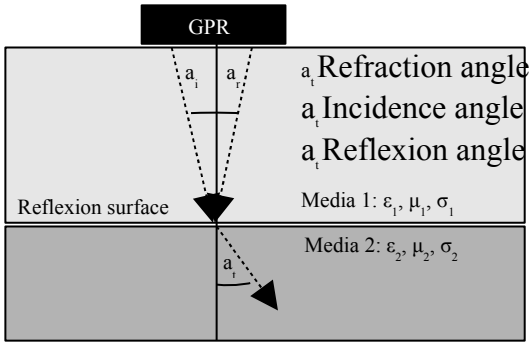

Fig. 2.6.

Chapter 3: GPR hardware and software

3.1. GPR Hardware

GPR's techniques are based on travel time and amplitude measures of the reflected wave of a short electromagnetic impulse transmitted through the pavement structure and successively reflected at the interfaces between layers. These interfaces are detected when the GPR wave match different materials, water content or density variation, etc. The GPR system have generally this three components:

- A generator that creates a single impulse of a given frequency and power.
- Antenna(s) for emit the impulse through the media and capture the reflected signal.
- A computer that digitalizes the received signal (sampling) and convert it into a format that can be processed.

Common radar antennas are divided into two categories: air-launched and ground-coupled antenna.

Ground-coupled antenna:

This type works at a center frequency that is in the 80-1500MHz range. Its main advantage is the greater depth penetration, in comparison with the another category. The main drawback is the low resolution at the first layer of the pavement.

The scan speed is also low, between 5 and 15 km/h (human step).

Main manufacturers are GSSI (New Hampshire, USA), Sensors & Software (Canada) and MALA (Sweden).

Air.launched antenna:

This one operates at the 500 – 2500 MHz range, usually 1000 MHz. The scan depth is typically between 50 and 90 cm, due to the high frequency values.

The name is because during the scan the antenna(s) is moved apart from the ground, let's say 30 – 50 cm. Therefore, the antenna can be mounted on a vehicle, so the scan speed (longitudinal axis, along the road) is much more greater than with the Ground-coupled antenna. It is normally to reach 60 or 70 Km/h. Main manufacturers are: GSSI (New Hampshire), Penetradar (NY) and Pulse Radar (Texas).

Fig. 3.1. Air-launched antenna. Vehicle mounted GPR.

Fig. 3.2. Antenna array.

3.2. GPR Software

The software available for road scan can be classified in four groups:

- Data acquisition unit
- Data elaboration unit (signal processing)
- Data visualization and interpretation unit
- Project and integrated analysis for the road unit

The main part of the acquisition software has been developed by the manufacturers of GPR systems. However, software packages for the storage and the quality control of the data are been spreading among researches, universities and enterprises. Advanced packages are necessary when Air-launched systems are used for the quality control of the pavement, as the scans must be reloable and the results of the GPR would be used after to determine variations and defects in the new scan. A very important property in the acquisition unit is the possibility of determine the spacial position, as modern systems need accurate information of the x, y , z coordinates.

GPR manufacturers offers also data elaboration systems, though most of them are developed to process data obtained with the Ground-coupled method for geological studies. Air-launched GPR systems give (usually) sharp signals, therefore the elaboration of the data is mainly done by the filtering algorithms of the received signal.

The interpretation and the visualization of the GPR systems are the scope of detect interfaces between layers, buried objects or singularities, transforming the GPR temporal scale into a spacial scale (specifically, depth). Many studies have been done with the goal of the automatic interpretation of the data obtained. However, the results are not been very engaging and moreover, these studies, have caused confusion among the road engineers. The reasons why these software suites doesn't work properly is because the roads, often, are historic structures damaged due to the passage of time and with longitudinal, vertical and transversal discontinuities. That's why data interpretation software, used by well prepared personnel together with other results (not only GPR, but also other kind of scan), make this option the unique valid solution for the road monitoring. The only cases in which the automatic interpretation seems to report correct thickness and permittivity values is in new pavements, free (or almost free) of defects.

One step beyond the new generation of GPR software is been developed with the integrated analysis of the road and with plan design programs, made for combined analysis of GPR data together with data made by other resources with the capability of determine the old road conditions and the parameters needed to create the new road or a rehabilitation program (Saarenketo, 1999). In the GPR scan of the roads, the outputs are represented in a numeric format or are visualized in longitudinal profiles or maps. Only when it's combined with another types of information the GPR is used to identify the potential cause of the superficial defects.

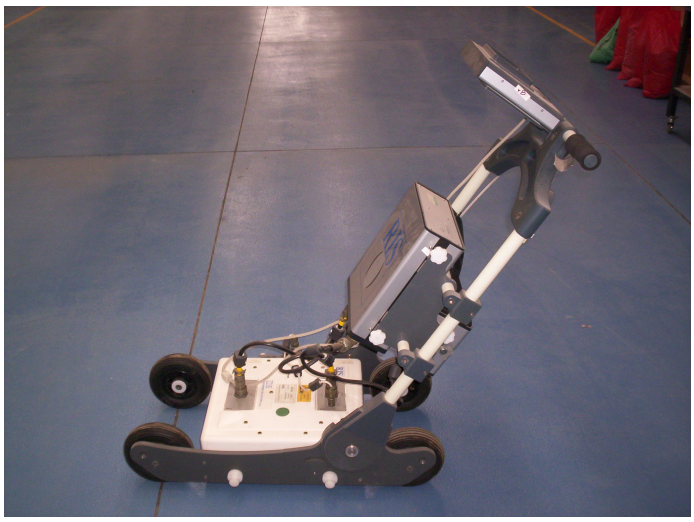

Fig. 3.3. The *new GPR at the "Università degli Studi Roma Tre" laboratory.*

Fig. 3.4. Acquisition unit.

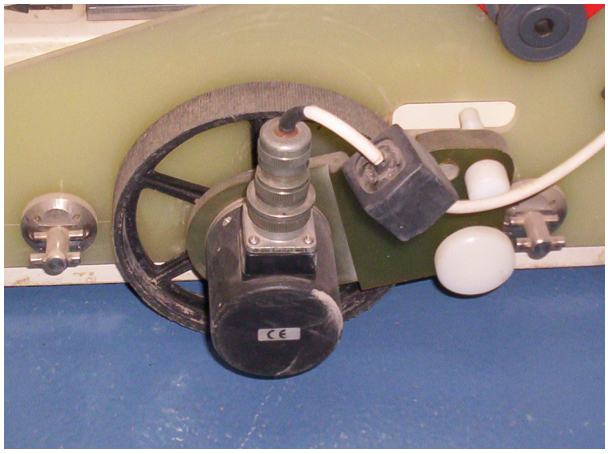

Fig. 3.5. Detail of the metric wheel.

In the pictures above there is a vision of the road laboratory with the instrumentation. The picture show the signal processing unit, composed by a computer and a battery. Then it is shown just the acquisition unit, that allows to shift the antenna from the ground. It is also shown the metric wheel that it is used to measure the extension of the scan and to allow the choose of the resolution that one want to use, based in the speed of the scan and in the type of study you want to follow.

3.3. The GPR configuration

The Ground Penetrating Radar, regarding the reception and transmission system, is available in two configurations: monostatic and bistatic (see picture below).

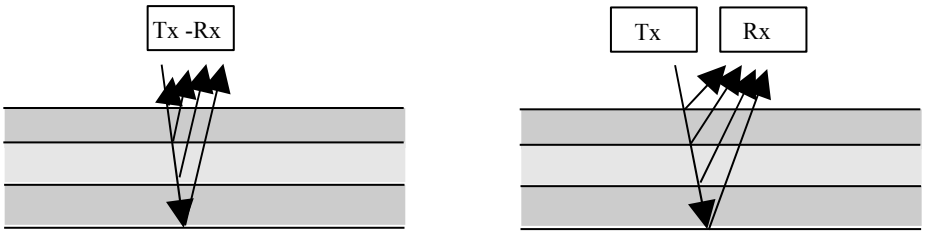

Fig. 3.6. Monostatic and bistatic configurations for the GPR

The monostatic configuration has one single antenna to emitting and receiving, in contrast with the bistatic type which has two different antennas. Generally, the measurement system (beyond the transmission/reception hardware) has a software for the management of these elements, a digital/analogical converser and a unit for the digital signal processing. Moreover, there are the visualization units for the raw and the processed signal. The signal processing is done by electronic filters in the frequency and spatial domain with the scope of:

- Remove the reflection of the first interface air/ground.
- Reduce the frequency components out of the selected frequency band (noise).
- Amplify the signal to reduce the attenuation effects.

Most of the GPR are directive, in other words, they emit following a preferential direction. Due the lobus emitting geometry, the radiation can reach targets that are not exactly settled on the vertical. Their reflexions will arrive later, as have to travel longer, so they will seem to be deeper. An example of this is the hyperbolic shape matching the reflecting points (as pipes, cobblestone, buried objects, landmines [6], etc). The ascending and descending branches are registered as the antenna passes through.

Fig. 3.7. Un−Processed Off−Lane GPR Data. Landmine detection

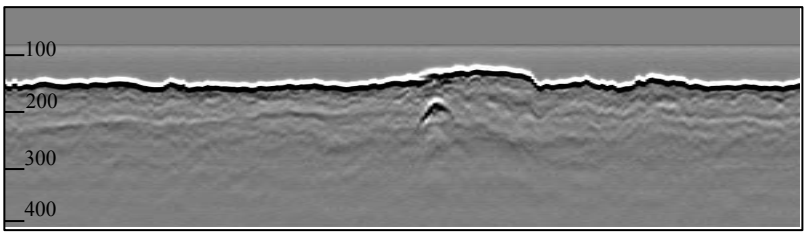

Fig. 3.8. SSAD−Processed Off−Lane GPR Data. Landmine detection

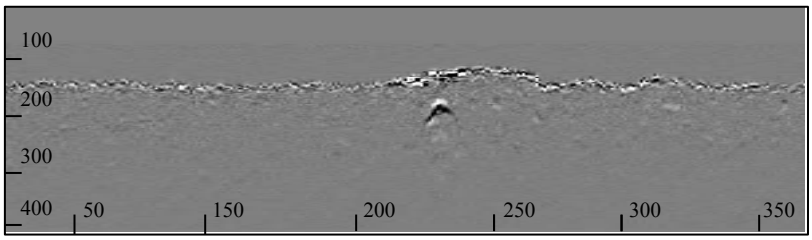

In general, at the pavement's applications, the vertical scans matches either the longitudinal or transversal direction of the road, getting the bidimensional radar map.

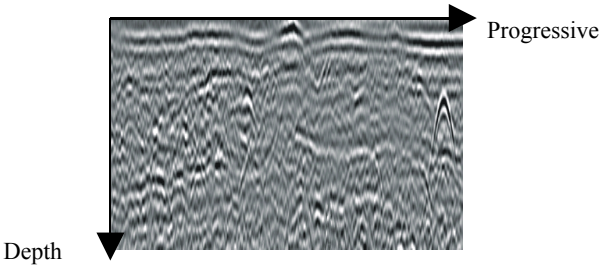

Fig. 3.9. Unprocessed radar map

At this chromatic maps -obtained moving the antenna along the surface-, the intensity of the color is proportional to the reflection signal in a given “grey scale”.

The GRP applications represents one of the fields with greater growth in the road engineering studies. One of the main reasons is the fact that the road network at the industrialized is already done by now, so the governments progressively focus on the maintenance and improvement on the standards on the network. At the same time there is the need for optimization the funds for this task, here it is why the strategies of maintenance and the rehabilitation techniques have the need for place the funds where we can take best profit. The GPR can certainly play an important role in this area, because is the only technology that can be used at high speed to get information of the pavement structure. As I said before, combining this methodology with other non-destructive tools we can get a powerful way for diagnose the current pavement problems and then select the best “repair” technique.

Chapter 4
The Layer-stripping algorithm

4.1. Introduction

The returned echoes of the GPR signal reflect the structure characteristic (pavement-layer thickness and the permittivity of each layer). We can estimate the delays and amplitudes of returned echoes reflected from the different dielectric media by matched filter and high resolution parameter estimation techniques (such as WRELAX [3]). Then the permittivity profile (layer thickness and permittivity) can be calculated from the estimation of the amplitude and the time delay $t_k(x)$. This is the layer stripping inversion approach [4][5].

The phases of the algorithm would be:

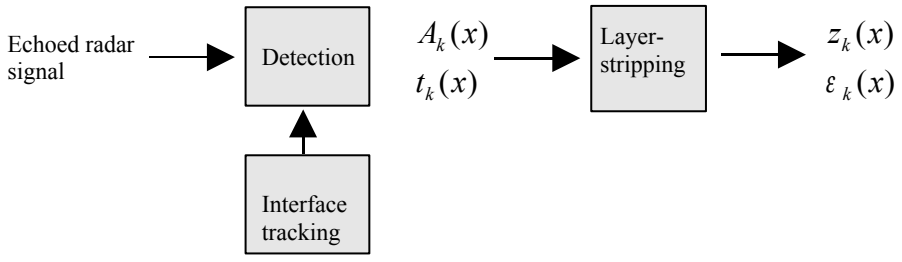

Fig. 4.1. Algorithm phases

In layer stripping inversion the permittivity profile is calculated from the estimation of the amplitude and the time delay of the detected radar echoes that refer to the th interface (plane wave approximation is usually understood in layer stripping approach). In monostatic GPR applications the amplitude and time of delay estimation is routinely performed on a scan-by-scan basis. However, the selection of inappropriate echoes, i.e., false alarms, will be discovered only during or after the layer stripping step. Such erroneous echoes provide the permittivity model building with a set of data points that, compared with the neighboring scans, contain some very large errors that can be visually appreciated from the lack of lateral continuity of permittivity values and/or interface profiles. The basic problem is that the interpretive step (echo detection) is performed with no reference to a physical model (physical models enter only when permittivity is calculated in layer stripping).

The lateral continuity of echoes that pertain to the same interface is not at all exploited in echo detection. Since interfaces can be considered as a sequence of laterally continuous echoes, the approach proposed is the tracking of interfaces. This approach reduces the probability of false alarms and leads to continuous interface profiles. In addition, layer stripping has the advantage of implicitly incorporating a constraint in the lateral variation of permittivity, this constraint being exploited by tracking the interfaces laterally.

Echo detection and interface tracking are two aspects exploited herein. The signal model is a superimposition of echoes of known (monopolar or bipolar) pulse shape $w(t)$

$$s(x,t) = \sum_k A_k(x) w[t - t_k] + n(x,t) \qquad (27)$$

additive term $n(x,t)$ with variance, or power, $\sigma_n^2 = E[n^2]$ takes into account zero mean noise and clutter. Pulse energy is $E_w = \sum_t w^2(t)$; for the *k*th echo energy is $A_k^2 E_w$ and signal to noise ratio is $SNR_k = A_k^2 SNR$ (where $SNR_k = \sigma_w^2 / \sigma_n^2$). System reverberation is assumed to be measured from free space experiment and removed before any processing. The pulse shape $w(t)$ differs from the transmitted pulse, mainly by the antenna response which is measured separately

by placing a flat metal plate at a known distance from the antenna. Pulse amplitude in normalized so that $|A_k| \leq 1$.

4.2. Echo detection and amplitude estimation

For each location, detection is a binary hypothesis testing between $H_0(x)$, that denotes no echo is present, and $H_1(x)$, an echo present in a subsequence of observations. Correlation receiver or **matched filter** is optimum for discriminating between desired echoes and white Gaussian noise $n(x,t)$.

⟹ A matched filter is obtained by correlating a known signal, or template, with an unknown signal to detect the presence of the template in the unknown signal. This is equivalent to convolving the unknown signal with a time-reversed version of the template (cf. convolution) . The matched filter is the optimal linear filter for maximizing the signal to noise ratio (SNR) in the presence of additive stochastic noise. Matched filters are commonly used in radar, in which a signal is sent out, and we measure the reflected signals, looking for something similar to what was sent out.

The filter is chosen to match the pulse shape $w(t)$

$$s^{(w)}(x,t) = \frac{1}{E_w}\int s(x,t+\zeta)w(\zeta)d\zeta \qquad (28)$$

estimation of echo (or echoes) time of delay (TOD) is obtained from local maxim of $s^{(w)}(x,t)$ evaluated within a pulse time window T. Normalization of matched filter guarantees, at least for isolated echoes, that $s^{(w)}(x,t_k(x)) \cong A_k(x)$ holds true.

This is the basic technical to get both time-delay and amplitude of the echo. In [4] we can find some improvements -as the sensitivity time control- to improve the SNR in matched filter, decrease the false alarm probability, etc.

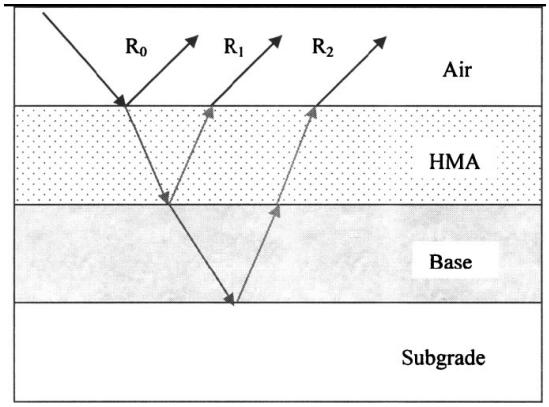

Fig 4.2. Interface reflexion in a typical pavement structure

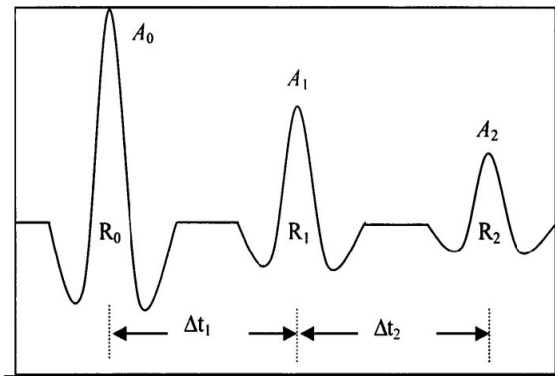

Fig 4.3. Radar scansion obtained from a pavement section

Sensitivity Time Control (STC)

The first moments of a reading echo, it has high power due to the nearby and the last readings usually have a significant power decreasing. The module responsible for correcting this is Sensitivity Time Control (STC) also called swept gain, anti-clutter control, suppressor or sea clutter control since it is commonly used to decrease the amplitude of nearby target that could be a false target caused by sea clutter. In calm seas this control is set to its minimum value. STC's main task is to detect close targets that might be obscured by sea clutter, but if it is set to its high value trying to remove sea-clutter, STC could remove small close targets too. The figure 1 shows

the kind of function used by the STC to correct sea clutter.

Sensitivity time-control circuits apply a bias voltage that varies with time to the IF amplifiers to control receiver gain. The Figure shows a typical stc waveform. When the transmitter fires, the stc circuit decreases the receiver gain to zero to prevent the amplification of any leakage energy from the transmitted pulse. At the end of the transmitted pulse, the stc voltage begins to rise, gradually increasing the receiver gain to maximum. In the ideal case the the receiver gain is proportionally to R^4. In the practice this course is frequently approached by the arising e function for the store of a condenser.

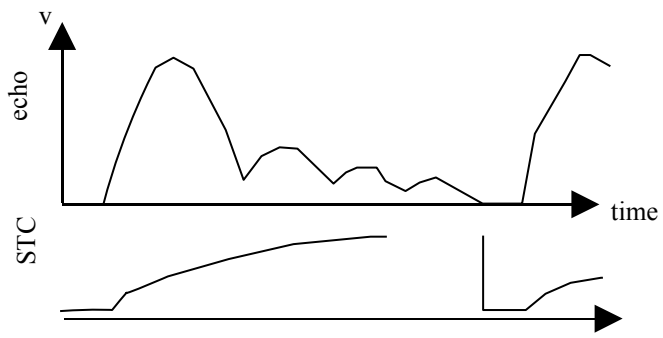

Fig. 4.4. Radar echo and STC signal applied

4.3. Interface tracking

Since interfaces can be considered as a sequence of laterally continuous echoes, the approach proposed is the tracking of interfaces. This approach reduces the probability of false alarms and leads to continuous interface profiles. In addition, layer stripping has the advantage of implicitly incorporating a constraint in the lateral variation of permittivity, this constraint being exploited by tracking the interfaces laterally. A finite-memory tracking filter is adopted for interface tracking after echo detection. For the *k*th interface, let $\hat{t}_k(x_i)$ be the predicted TOD at location x_i; the tracked TOD $\hat{t}_k(x_i)$, selected from among the detected echoes, is the one with the largest

amplitude within a search window T_s around $\hat{t}_k(x_i)$. The predicted time is obtained using the $\alpha - \beta$ tracking filter

$$\hat{t}_k(x_i) = \hat{t}_k(x_i - 1) + \alpha\,[t_k(x_i - 1) - \hat{t}_k(x_i - 1)] + \Delta t_k(x_i - 1) \qquad (29)$$

where the time variation $\hat{t}_k(x_i)$ is estimated with the finite-memory algorithm

$$\Delta t_k(x_i - 1) = \Delta t_k(x_i - 2) + \beta\,[t_k(x_i - 1) - \hat{t}_k(x_i - 1)] \qquad (30)$$

The interface selection depends on the tracking initialization: $t_k(x_0) = \hat{t}_k(x_0)$ and $\Delta t_k(x_0) = 0$. Coefficients α and β should be selected as a compromise between low tracking noise (small α and β) and good tracking capability of rapid interface variations (large α and β). The value of T_s also depends on the choice of tracking coefficients. The tracking of echo delay with larger variations needs large T_s while small T_s increases the misses of interfaces with rapid time-variations. Tracking of multiple interfaces is performed iteratively since each iteration corresponds to tracking of only one interface. The interfaces already tracked in previous iterations are removed from detected data to avoid multiple tracking of the same interface

In order to see the Matlab implementation of the step A and B (phase 1: detection) please go to Appendix A.

4.4. Layer-stripping

The permittivity profile $\varepsilon(x_i, z)$ and interface depth $z(x_i)$ are obtained from the estimation of the interface TODs $t_k(x_i)$ and amplitude $A_k(x_i)$ derived from monostatic GPR measurements $s(x_i, t)$.

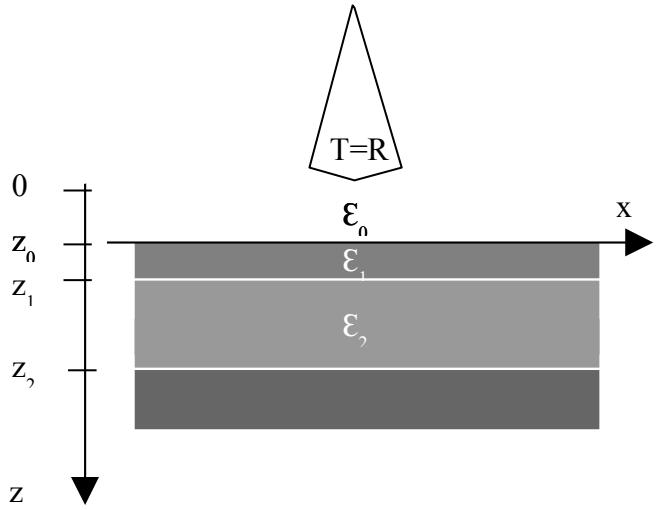

Fig. 4.5. Geometry of monostatic radar.

Let the estimated echoes be sorted for increasing TOD (i.e., $t_1(x_i) < t_2(x_i) < \ldots < t_{K_i}(x_i)$ the permittivity values and interface thicknesses are estimated iteratively from the following relationships:

$$z_{k+1}(x_i) = z_k(x_i) + \varepsilon^{-1/2}(x_i, z_{k+1})[t_{k+1}(x_i) - t_k(x_i)]c/2 \qquad (31)$$

$$A_k(x_i) = r_k \rho_k(x_i) \cdot \prod_{q=0}^{k-1} \tau_k(x_i) \qquad (32)$$

given by the reflection (ρ) and transmission (τ) coefficients for plane wave at each boundary. Equivalent attenuation set $\{r_k\}$ depends on the specific application and is evaluated during the GPR calibration.

For that calibration we need a sample core of the ground we are studying, so we have a set of z_k values. Then, for that k sweep we have all the data needed and we can isolate the 'equivalent attenuation set' $\{r_k\}$ and then used as a input for the algorithm.

I also created a mini-application for that calculation. (Appendix B.1)

The normal incidence reflection coefficient for downward traveling wave is:

$$\rho_k(x_i) = \frac{\varepsilon^{1/2}(x_i, z_k) - \varepsilon^{1/2}(x_i, z_{k+1})}{\varepsilon^{1/2}(x_i, z_k) - \varepsilon^{1/2}(x_i, z_{k+1})} \tag{33}$$

the two way transmission coefficient at *k*th interface is:

$$\tau_k(x_i) = \frac{4\varepsilon^{1/2}(x_i, z_q)\varepsilon^{1/2}(x_i, z_{q+1})}{[\varepsilon^{1/2}(x_i, z_q) + \varepsilon^{1/2}(x_i, z_{q+1})]^2} \tag{34}$$

In the air, the relative permittivity is and the $\varepsilon(x_i, z_0) \equiv 1$ propagation velocity is c = 30cm/ns; $t_0(x_i)$ and $A_0(x_i)$ are the TOD and the amplitude of the air ground interface; the known antenna distance from the pavement surface $z_0(x_i)$ is useful to set the TOD reference for deeper ($k \geq 1$) interfaces as $t_0(x_i) = 2z_0(x_i)/c$.

Putting all together in a diagram:

$$A_k = \begin{pmatrix} A_{00} & A_{01} & & A_{0n} \\ A_{10} & A_{11} & & A_{10} \\ & & \ddots & \\ A_{n0} & & & A_{nn} \end{pmatrix} \qquad \begin{pmatrix} \varepsilon_{00} & \varepsilon_{01} & & \varepsilon_{0n} \\ \varepsilon_{10} & \varepsilon_{11} & & \varepsilon_{10} \\ & & \ddots & \\ \varepsilon_{n0} & & & \varepsilon_{nn} \end{pmatrix} = \varepsilon_k$$

$$\varepsilon_k = f(A_k)$$
$$z_k = f(t_k, \varepsilon_k)$$

$$t_k = \begin{pmatrix} t_{00} & t_{01} & & t_{0n} \\ t_{10} & t_{11} & & t_{10} \\ & & \ddots & \\ t_{n0} & & & t_{nn} \end{pmatrix} \qquad \begin{pmatrix} z_{00} & z_{01} & & z_{0n} \\ z_{10} & z_{11} & & z_{10} \\ & & \ddots & \\ z_{n0} & & & z_{nn} \end{pmatrix} = z_k$$

Fig. 4.4. Layer-stripping algorithm matrix diagram

4.5. Matlab implementation

The Matlab implementation of the algorithm introduced before is based on:

1. Obtain amplitude of reflexion and time delay matrix's

- This is given by the embedded software of the acquisition unit (raw data). To obtain the time delay matrix we apply the interface tracking algorithm explained above. This approach reduces the probability of false alarms and leads to continuous interface profiles.

$$A_k = \begin{pmatrix} A_{00} & A_{01} & & A_{0n} \\ A_{10} & A_{11} & & A_{10} \\ & & \ddots & \\ A_{n0} & & & A_{nn} \end{pmatrix} \qquad t_k = \begin{pmatrix} t_{00} & t_{01} & & t_{0n} \\ t_{10} & t_{11} & & t_{10} \\ & & \ddots & \\ t_{n0} & & & t_{nn} \end{pmatrix}$$

- Let's assume A_{00} is value in volts of the first sample (z = 0 m) of the reflected signal (trace #0, x =0m).
- A_{n0} would be the last sample ($z = b$ m) of the first trace (the deepest sample of the first trace).
- One we have the values of the first trace, we move on the x-axis the GPR hardware in order to obtain the sampling of the second trace ($x = x + d$ m).
- A_{01} would be the first sample of the second trace; A_{n1} the deepest sample of the second trace.
- Going on with the scan we arrive to the last trace (A_{in}) ($x = a$ m).
- The matrix of time delays t_k it's simply the corresponding values of time delay of each amplitude of reflexion sample A_{ij} . It's clear then that:

$$t_{y0} \approx t_{y1} \approx \cdots \approx t_{yn} \quad \text{and that} \quad t_{0x} < t_{1x} < \cdots < t_{nx}$$

Where a is the total displacement in meters from the first trace to the last one.

b Would be the deepest sample of a scan. Note that $a * b$ is the size of our matrix.

d Is the relative deplacement between scans (radar shoots), and c is space/time between samples

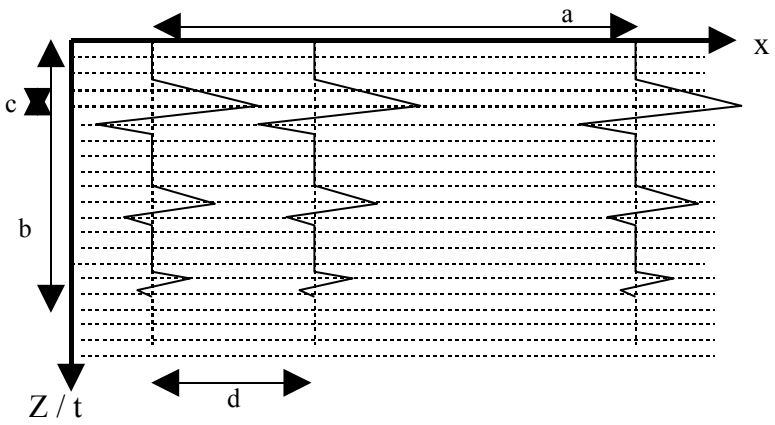

Fig. 4.5. Matrix parameters from scan

2. Insert the data and process it iteratively: Layer-Stripping algorithm

- Once we have both matrix of amplitude reflexion and time delay, we insert them into the algorithm by a simple file browsing with the user-friendly interface I created so.

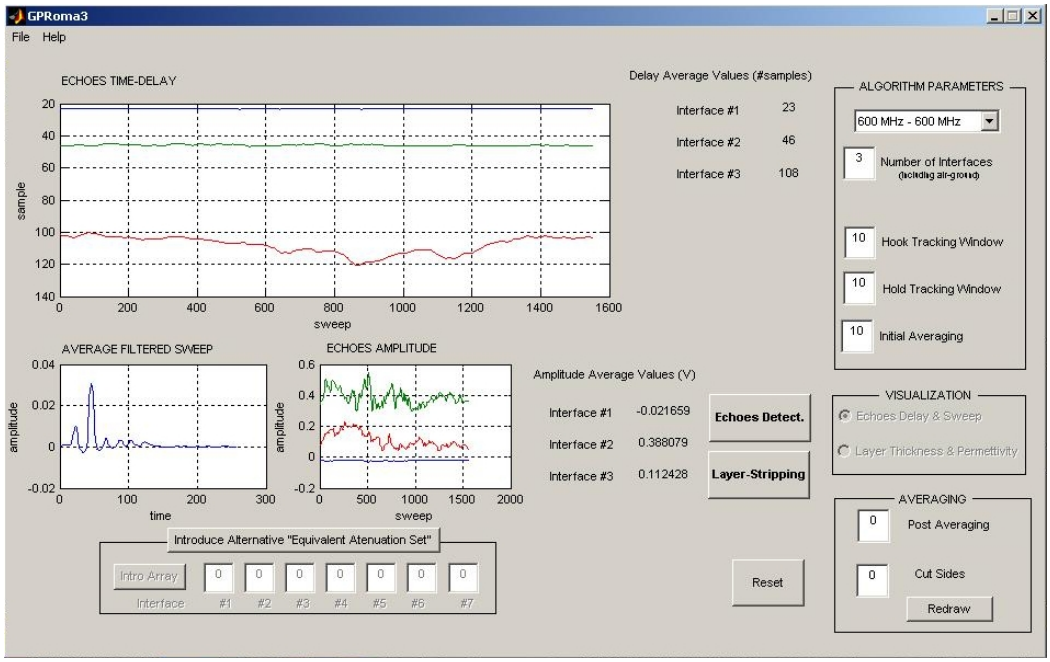

Fig. 4.6. GPRoma3 application screen shot

- Introduce the parameters needed for processing, as frequency, etc, etc.
- Press 'Echoes Detect.' button (result in the screen shot above).

- Once 'Echoes Detect.' process is finished (progress bar 100%), press 'Layer-Stripping' button (the view of the graph will change into the one at *Fig.4.8*).
- Internally, the application will process column by column like this, from top to bottom:

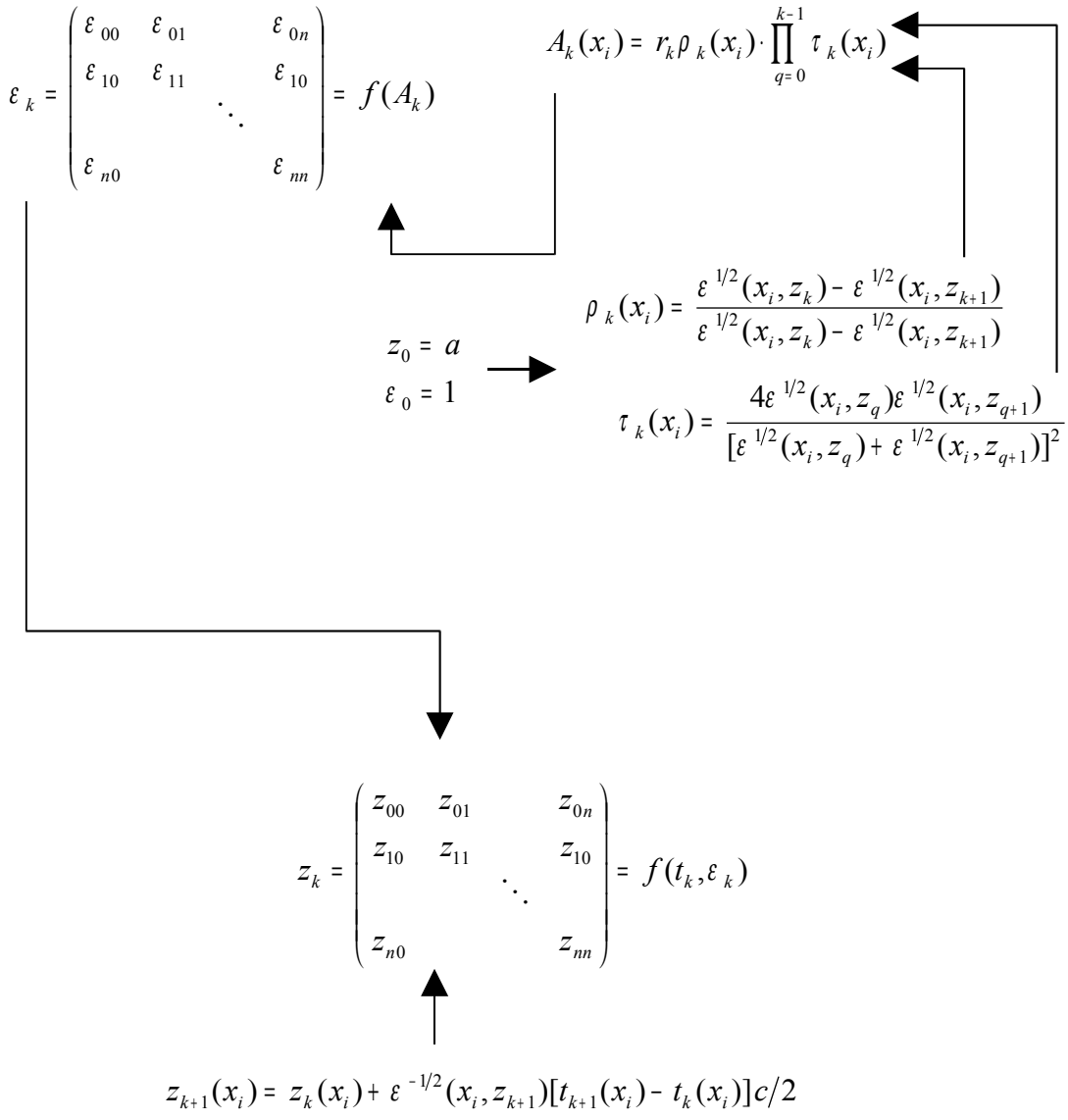

Fig. 4.7. Layer-stripping matrix algorithm and equations involved in.

3. Graphic representation

- At this point we have both thicknesses and permittivity matrix's. Now we want to represent them in its physic interpretation way, it is, as a section of the ground we are studding.
- In the z-axis we will have the thickness of each layer in x-axis continuity.
- Moreover, we have the value of permittivity for each pair (x_i, z_j). That value will be colored in a chosen metric color scale. The lighter color of our palette as the lowest value of permittivity we have in the scan and the darkest for the higher value.
- One drawback we have is that our values of permittivity $\varepsilon = (x_i, z_j)$ are constant in a whole layer, it is, $\varepsilon = (x_i, z_j) = (x, z_{k+1} - z_k)$. That is because we do not have the means to know the values of permittivity in every single point z in a given layer, that is, between two interfaces.
- Taken in account all that it is been explained in this point. The graphic out of the application look like this:

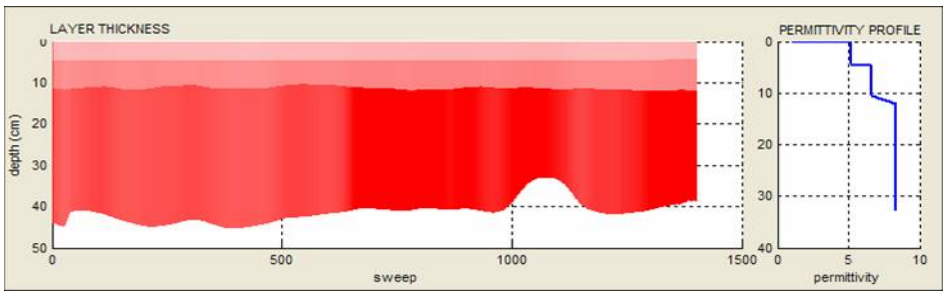

Fig. 4.8. Graphs out of the application for a given section of a road. Left, layer thickness. Right, permittivity profile.

- In addition to the section graph mentioned above it is displayed a permittivity profile graph clearly related to the former. The graph represent the average value of permittivity for each layer.
- The matrix's are represented like that with complex iterative expressions the Matlab code.
- Once we have the visual representation of the analyzed data, the application outs a text file with the main values of the scan: Average permittivity, average velocity (m/s) and average thickness (cm) in each detected layer.

```
AVERAGE LAYER VALUES
Average permettivity in layer  1  =  5.17227
Average velocity in layer  1  =  1.31911e+008 m/s
Average thickness in layer  1  =  4.62499 cm
-----------------------------------------------------
Average permettivity in layer  2  =  6.58567
Average velocity in layer  2  =  1.16902e+008 m/s
Average thickness in layer  2  =  6.76197 cm
-----------------------------------------------------
Average permettivity in layer  3  =  8.32608
Average velocity in layer  3  =  1.03968e+008 m/s
Average thickness in layer  3  =  29.7092 cm
-----------------------------------------------------
```

Fig. 4.9. Screen shot of the text file out of a scan.

- Go to Appendix C to find the help file of the application.

Chapter 5

Experimental verification

5.1. Pavement types. Basic structural elements

Pavement Types

Hard surfaced pavements are typically categorized into flexible and rigid pavements:

- *Flexible pavements*. Those which are surfaced with bituminous (or asphalt) materials. These types of pavements are called "flexible" since the total pavement structure "bends" or "deflects" due to traffic loads. A flexible pavement structure is generally composed of several layers of materials which can accommodate this "flexing". This is the kind of pavement used (usually at roads).

- *Rigid pavements*. Those which are surfaced with "portland" cement concrete (PCC). These types of pavements are called "rigid" because they are substantially stiffer than flexible pavements due to PCC's high stiffness. Usually it is used at places where it has to stand a big weight over, like a plane parking or something like that.

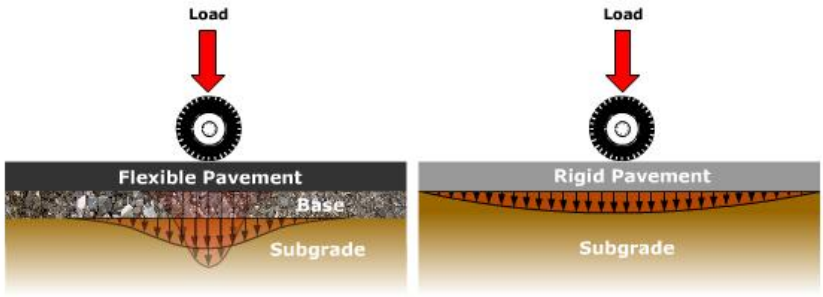

Fig. 5.1. Rigid and flexible pavement load distribution

Each of these pavement types distributes load over the subgrade in a different fashion. Rigid pavement, because of PCC's high stiffness, tends to distribute the load over a relatively wide area of subgrade (see *Fig. 5.1* -right). The concrete slab itself supplies most of a rigid pavement's structural capacity. Flexible pavement uses more flexible surface course and distributes loads over a smaller area. It relies on a combination of layers for transmitting load to the subgrade (see *Fig. 5.1* -left),

Flexible Pavement Structure

Flexible pavements are so named because the total pavement structure deflects, or flexes, under loading. A flexible pavement structure is typically composed of several layers of material each of which receives the loads from the above layer, spreads them out, then passes them on to the layer below. Thus, the further down in the pavement structure a particular layer is, the less load (in terms of force per area) it must carry

Basic Structural Elements

Material layers are usually arranged within a pavement structure in order of descending load bearing capacity with the highest load bearing capacity material (and most expensive) on the top and the lowest load bearing capacity material (and least expensive) on the bottom. A typical flexible pavement structure (see *Fig. 5.2*) consists of:

- *Surface Course*. The layer in contact with traffic loads. It provides characteristics such as friction, smoothness, noise control, rut resistance and drainage. In addition, it prevents

entrance of surface water into the underlying base, subbase and subgrade (NAPA, 2001). This top structural layer of material is sometimes subdivided into two layers: the **wearing course** (top) and **binder course** (bottom). Surface courses are most often constructed out of HMA.

- *Base Course*. The layer immediately beneath the surface course. It provides additional load distribution and contributes to drainage. Base courses are usually constructed out of crushed aggregate or HMA.
- *Subbase Course*. The layer between the base course and subgrade. It functions primarily as structural support but it can also minimize the intrusion of fines from the subgrade into the pavement structure and improve drainage. The subbase generally consists of lower quality materials than the base course but better than the subgrade soils. A subbase course is not always needed or used. Subbase courses are generally constructed out of crushed aggregate or engineered fill.

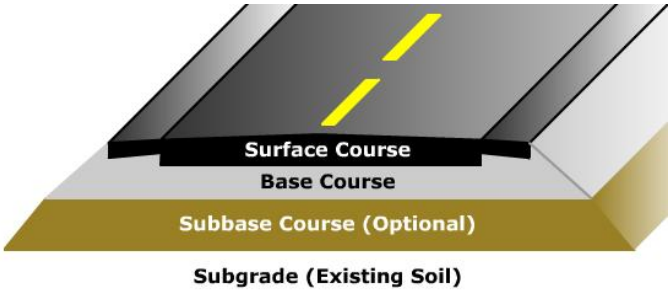

Fig. 5.2. Typical flexible pavement structure

5.2. Experimental verification: the Carpiano (Milano) data

To do the first experimental verification of the algorithm I had a set of data from a previous thesis: “Analisi del degrado sttruturale di pavimentazioni stradali con georadar", by Silvia Pensa at Università degli studi Roma Tre. I took some of the sets of data of several meassures were made at that thesis and I tried to get the same measures of depth, permittivity and thickness of the pavement with my algorithm implemented at Matlab.

Here below there is the thickness and permittivity measurements of the piece of pavement i took to do the verification, as well as a cross-section diagram.

I had the outputs files of the Geo Radar, which are matrix of numbers, amplitudes (V) of reflexion. I put these files as inputs at my Matlab algorithm and I tried to see if the measurements of my program were the same as the measurements made *in situ*.

	Thickness (cm)	Permittivity
Wearing course	4,8	*6 (12,55 cm)
Binder	7,75	
Base	22,75	*8

Fig. 5.3. Measurements for the section I.I of pavement

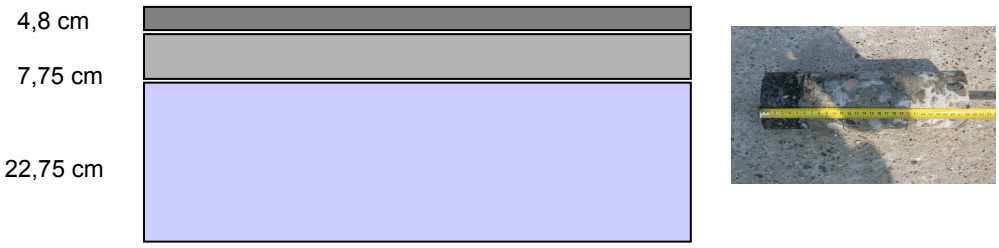

Fig. 5.4. Layer-thickness diagram of the section I.I. and photo of a sample core.

5.2.1. 600 - 600 MHz GPR configuration

This configuration -600 MHz TX, 600 MHz RX- allows you to go deeper in the ground. Let's say it is possible to reach till 2 or 3 meters of deepness. As a drawback, we have less resolution. This is a classic agreement at radar and teledetection: range VS resolution.

This problem with the resolution at this configuration, doesn't allow us to distinguish the two first layers, wearing and binder course, which use to have only a few centimeters of thickness (around 5 cm). So they both appear in one layer. It also happen that usually wearing and binder course have a very similar permittivity, therefore the interface between layers does not produce a big reflexion, increasing the difficult to detect each layer.

Here bellow there is a shot of the graphs given by the algorithm in Matlab. At the left side we have a 3D representation of the cross section of the road. On the y-axis there is the deepness. The x-axis is the axis that goes longitudinally on the direction of the scan. In this cases the x-axis does not have units, as is measured in 'sweeps'. To transform it into a longitude unit (as meters), you just have to multiply the number of sweep by the distance between sweeps. Usually, the longer the total scan, the greater the distance between sweeps. In the case of road monitoring (not object detection, for example) should be enough using a 10% of the total longitude as the distance between sweeps.

Then, colored in different shades of red, we have the different values for the permittivity. Those parts with the lighter red are those parts of the pavement structure with smaller values of permittivity. As a clear example, you can see that the top is all in light red, drawing an interface between layers. This is because the whole layer has a smaller value of permittivity. The bottom part is in a darker red, but with its shades. As a remembering, little differences in the humidity level of the road (for example), gives different values of permittivity at that part of the structure.

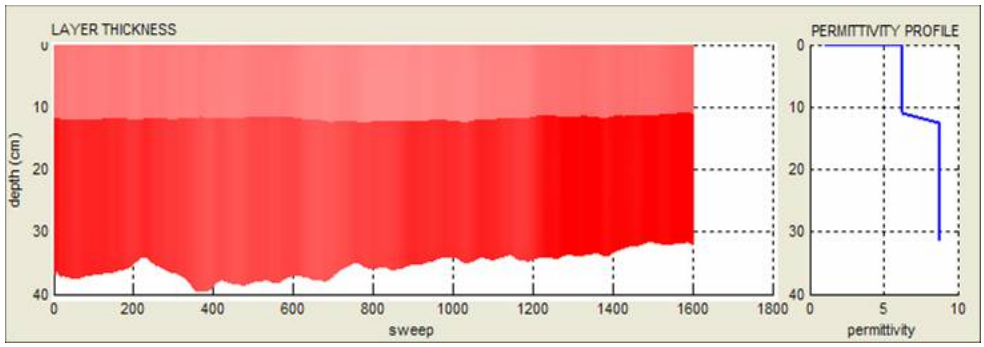

Fig. 5.5. 600-600 MHz. configuration plot out of the algorithm. Section I.I. from the Carpiano data.

```
AVERAGE LAYER VALUES
Average permettivity in layer  1  =  6.28093
Average velocity in layer  1  =  1.19704e+008 m/s
Average thickness in layer  1  =  11.8793 cm
-----------------------------------------------------
Average permettivity in layer  2  =  8.79027
Average velocity in layer  2  =  1.01186e+008 m/s
Average thickness in layer  2  =  23.4837 cm
-----------------------------------------------------
```

Fig. 5.5. 600-600 MHz. configuration text file of the algorithm. Section I.I. from the Carpiano data.

	Real Thicknesses	Real Permittivity	Measured Thicknesses	Thicknesses Error	Measured Permittivity	Permittivity Error
Wearing	4.8 cm	~ 6 (12.5 cm)	11.8 cm	0.7 cm (6%)	6.3	0.3 (5%)
Binder	7.7 cm					
Base	22.7 cm	~ 8	23.5 cm	0.8 cm (4%)	8.8	0.8 (9%)

Fig. 5.6. 600-600 MHz. configuration comparative table between real and measured data, section I.I Carpiano data..

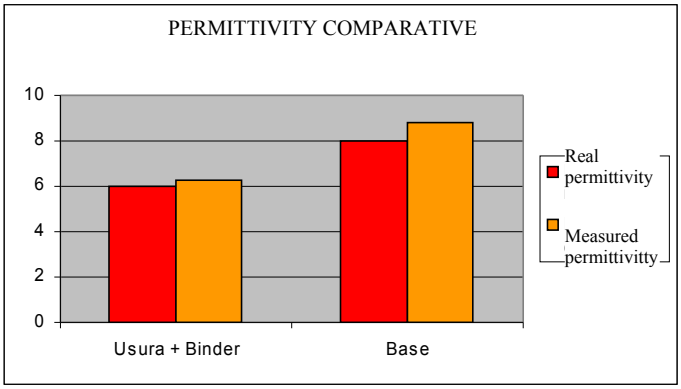

Fig. 5.7. 600-600 MHz. configuration comparative graph between real and measured data, section I.I Carpiano data.. Permittivity.

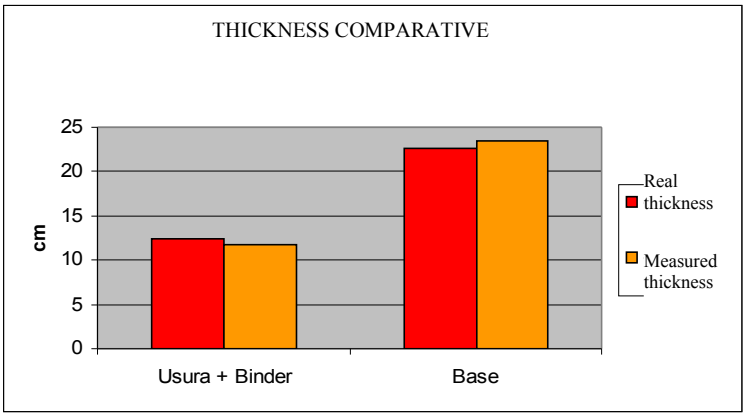

Fig. 5.8. 600-600 MHz. configuration comparative graph between real and measured data, section I.I Carpiano data.. Layer thickness.

This results for the 600-600 MHz configuration prove how useful and accurate can be the GPR -with a proper signal processing behind- for road monitoring, ground characterization, thickness and permittivity profiling, etc.
With the mentioned configuration we have got:

- ✓ Thicknesses estimation: Error < 6%
- ✓ Permittivity estimation: Error < 9%

The main drawback for this configuration is the fact that we don't have enough resolution to distinguish the wearing course and the binder layer, as the thickness of the former is too small for this 600-600 MHz configuration.

5.2.2. 1500 - 1500 MHz GPR configuration

For this configuration we expect to have more resolution -so hopefully we will be able to detect the first layer, wearing course-, and probably less range or deepness, as higher frequencies get attenuated strongly.
Also we have to see how accurate is this configuration, in comparison with the 600-600 MHz.
Following there are all the plots and data obtained from the application.

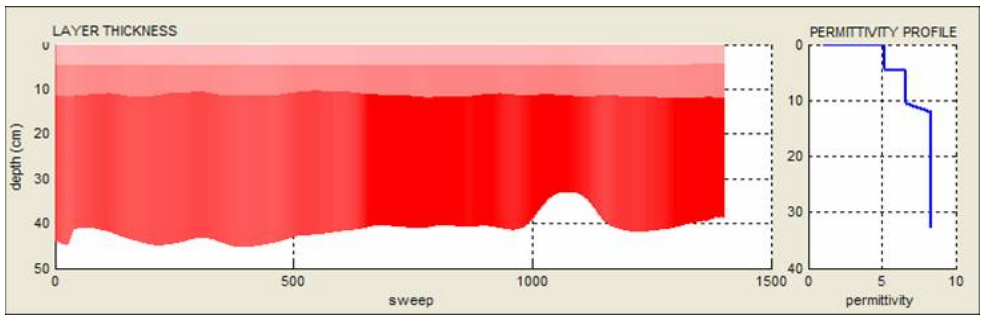

Fig. 5.9. 1500-1500 MHz. configuration plot out of the algorithm. Section I.I. from the Carpiano data.

```
AVERAGE LAYER VALUES
Average permettivity in layer  1  =  5.17227
Average velocity in layer  1  =  1.31911e+008 m/s
Average thickness in layer  1  =  4.62499 cm
-----------------------------------------------------
Average permettivity in layer  2  =  6.58567
Average velocity in layer  2  =  1.16902e+008 m/s
Average thickness in layer  2  =  6.76197 cm
-----------------------------------------------------
Average permettivity in layer  3  =  8.32608
Average velocity in layer  3  =  1.03968e+008 m/s
Average thickness in layer  3  =  29.7092 cm
-----------------------------------------------------
```

Fig. 5.10. 600-600 MHz. configuration text file of the algorithm. Section I.I. from the Carpiano data.

	Real Thicknesses	Real Permittivity	Measured Thickness	Thickness Error	Measured Permittivity	Permittivity Error
Wearing	4,8 cm	~ 6	4,7 cm	0,1 cm (2%)	5,2	0,05 (0,8%)
Binder	7,7 cm	(12,5 cm)	6,8 cm	0,9 cm (11%)	6,7	
Base	22,7 cm	~ 8	29,7 cm	7 cm (23%)	8,3	0,3 (3%)

Fig. 5.11. 1500-1500 MHz. configuration comparative table between real and measured data, section I.I Carpiano data..

For this configuration we have obtained:

- ✓ Thicknesses estimation: Error < 23%
- ✓ Permittivity estimation: Error < 3%

As we see, the error in the thicknesses estimation is greater than what we should expect. Having a look at the table *Fig. 5.11.*, at the thicknesses error column we notice that the error grows layer after layer:

- ✓ Wearing thickness estimation: Error = 2% (4,8 cm depth)
- ✓ Binder thickness estimation: Error = 11% (12,5 cm depth)
- ✓ Base thickness estimation: Error = 23% (35,2 cm depth)

It is clear to see that as the deeper is the layer, the greater the error at the estimation.
There is no doubt that something in the algorithm should be revised in order to fix this error.
My opinion it is something that has to do with the STC (sensitivity time control), it is, the correction we do on the returned signal in order to amplify far distant echoes.
Unfortunately my thesis time is finishing, so this remains as a further work to do.

Chapter 6
Practice application: Linate Airport mission, Milano (July 2006)

6.1. Introduction

On July of 2006, the University of Roma Tre was asked by the Politecnic University of Milano for doing an experiment at the Linate Airport (Milan).

It was about doing an experimental verification with the GPR of the works of the installation of a new enlightenment system on some of the landing runways of the airport. This new enlightenment was going to be installed with no-dig technology, it is, without doing any open-air bug. All the wires and the lights will be placed by doing a tunnel all along the landing runway. The advantages of this technologies are clear. It is much more faster and easier to put a cable under the ground (let's say a 100 meters cable) by doing a tunnel rather than open a 100 meters bug, put the cable and then close it all again. This efficiency is specially appreciated in a case such an airport, where building works can affect in a very negative way the proper work of the place.

The negative aspects of this kind of operation is that it is not well estimated what kind of impact can have the tunnel of the ground structure. The main problem would be that for doing the tunnel it is required to infiltrate thousands of liters of water, in order to soften up the ground as well as to cool the drill. This water does not remain nearby the tunnel (as the ground is not porous and liquid can travel through), it goes infiltrating through the ground structure, possibly damaging it. As

ground gets wet it losses some bearing capacity. If we think that landing runways and parking squares for planes have to carry tons of weight, we realize that bearing capacity is a crucial matter. The GPR verification was all about measuring the impact of the water infiltration on the ground structure. With that purpose, longitudinal and transversal scans were made with the GPR before, during and after the tunnel operation.

6.2. Measurements and procedure

Once we arrived to the landing runway where the operations were taking place we start taking measures and guessing where will be the best lines to pass the GPR over.

At the *Appendix A* there are all the diagrams that illustrates the work we made there with the corresponding explanation: I.e. scan before/after/during the operation, date, etc..

At all the different locations where we made scans, we made both transversal and longitudinal scans, as it is clear at the diagrams.

Next I would like to show some pictures that will illustrate pretty much the whole operation:

Fig. 6.1. Tunnel point of entry

Fig. 6.2. Tunnel operation

Fig. 6.3. Extraction of a sample core

Fig. 6.4. Sample core

Fig. 6.5. Prof. A. Benedetto and Spartaco adjusting the GPR

Fig. 6.6. Transversal scan

Fig. 6.7. Data from GPR to PC

Fig. 6.8. Light installed at the runway

6.3. Conclusions

As this mission took place in July and I had to write and submit the thesis right after the summer, I could not study the whole data we got at Linate Airport. However, I select some relevant scan to extract the data and process it with the application I designed.

These relevant scans were taken from the set of scans at the *Figure 3* and *Figure 5*. The scans at the Figure 3 were taken before the tunnel operation was made and the ones from the Figure 5 after the operation was made.

In particular here we have the graphics out of the transversal scan number 13.
These two first graphics were taken before the drill pass by the cross-section 13th:

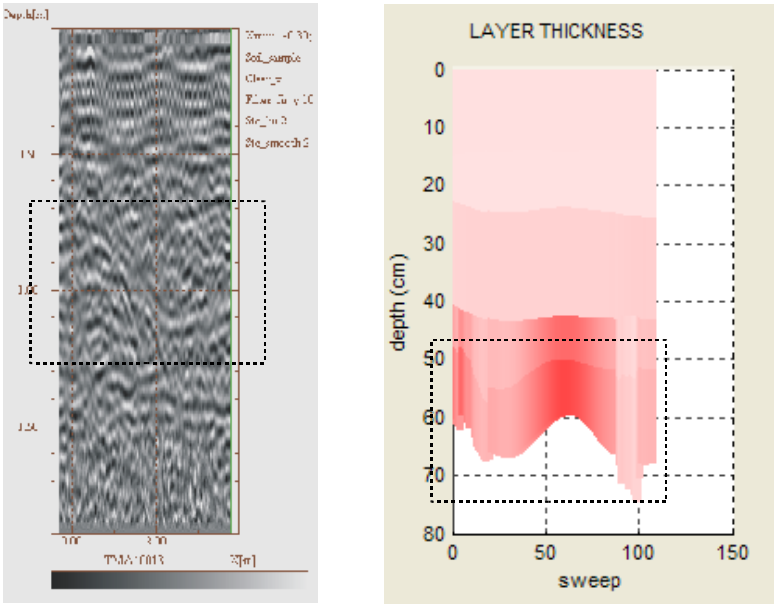

Fig. 6.9. Cross-section 13th scan (Appendix A, Folder AERO3, TMA 0013)

The image at the left side is the one that the GPR integrated software print out. As I explained before, the gray scale represents the intensity of the signal (V) at that point, it is, the intensity of the reflexion. The whiter is the point, the greater is the value of the reflexion there.

On the right side there is the graph that comes out of the algorithm I designed. As well as the GPR integrated software graph, the depth (m) is on the y-axis, while the permititivity value is colored in red. The darker the red, the greater the permititivity at that point. The values on the graph match

values of permittivity from 5-6 (lighter red, top) to 10-12 (darker red, bottom). That are normal values of permittivity for that soil. Also the layer thickness does not reveal any anomaly. There is the first layer of 20cm thickness approx. (surface). Then a second from 20cm depth to 40cm (base). And at the bottom there is the subgrade.

Note that the images correspond to the same cross-section as it is noticeable the same shapes in both pictures. That are the interfaces between different permititivity areas. In this section, the top interfaces (from 0 to 40 cm of the depth approx.) are almost flat, while the bottom interfaces drawn some kind of curve.

The following graphs correspond to the same place after the tunnel operation passes through that cross-section (13th):

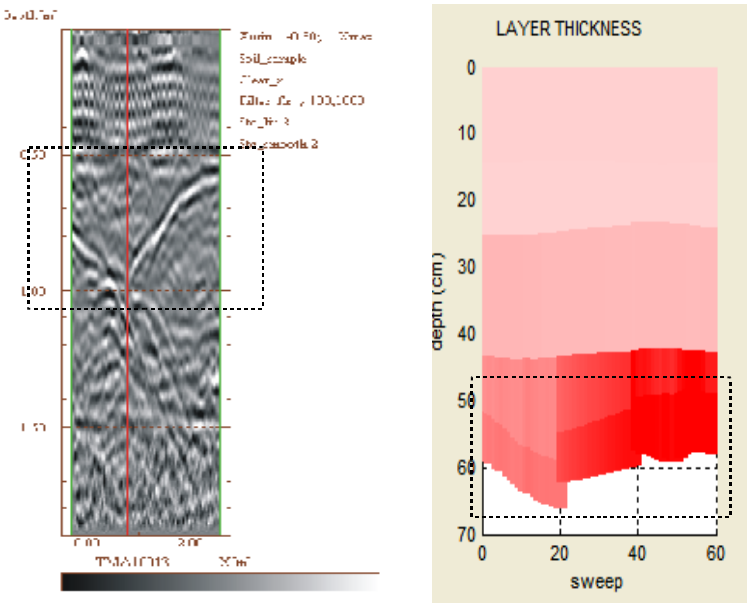

Fig. 6.10. Cross-section 13th scan (Appendix A, Folder AERO5, TMA 0013)

On the top layers everything seems normal and yet equal in comparison with the scans made before the tunnel crosses that section. However, if we pay attention to the bottom layer (subgrade) we see that the interface at 60cm depth approx. has change. Two aspects must be analyzed:

1 – The shape of the bottom interface is different than the *Fig. 6.9.* It is distinguishable 2 south-north hyperbolas going from bottom to top (blue/yellow dashed lines) .

2 – Endarkment of the bottom layer (darker red). That means the permititivity values at that layer has increase. Looking the table that matches the intensity of red and the permititivity at that point I noticed an increase of almost 8 units, from 10-12 (before the operation) to 20 approx after the tunnel was made.
The following picture reveal what happened.

Fig. 6.11. Water coming up to the surface trough a joint

As we expected, the water that the top of the drill injects does not remain on the immediate surrounding but it goes infiltrating through the ground, soaking a big area. Indeed, that picture was taken almost 5 meters from where the hole/drill was made.

All that water emaning from where the drill passed soaked a big area around the tunnel. As water has a dielectric constant of 80, when it mixes with ground the result is an increase of dielectric constant of the soil. In this case, the bottom surface had a D.C. of 10-12 and after mixing the water it increased till 20 approx

Also at the graphs A/B we noticed some kind of hyperbola shapes, from bottom to ground. That is nothing but the *paths* that water followed in his way to the surface, as we see in the picture 44.
What kind of impact can have all that water in the ground?
At the moment I finished my work the concussions and all the analysis about the Linate Airport where not finished.

However, that analysis is work of ant civil engineer. My work there was to design and implement a tool to help the professionals at the field of civil engineering. It is just one more tool added to the

collection of tools they have already. Therefore, my software must not be used as an unique tool to analyze, but together with other resources to compare and contrast the different data obtained from each device.

APPENDIX A: Linate Airport scan diagrams and photos

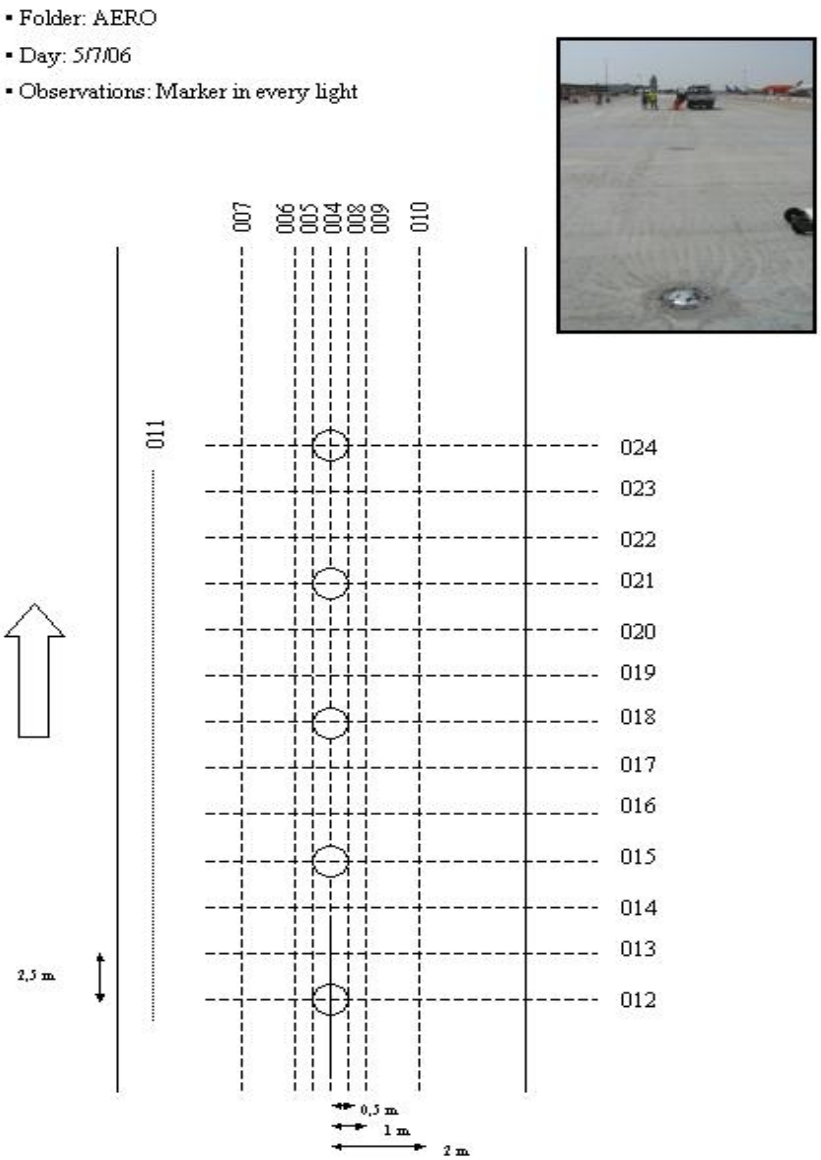

- Scan after the enlightenment operation was made.
- 7 longitudinal scans. 1 of them just over the lights line and 3 at right and left side, symmetrically. 0.5, 1 and 2 meters from the central line.
- 1 extra longitudinal scan at several meters from the operation was made in order to measure the initial ground before any operation was made
- 12 transversal scans. 2.5m between scans.

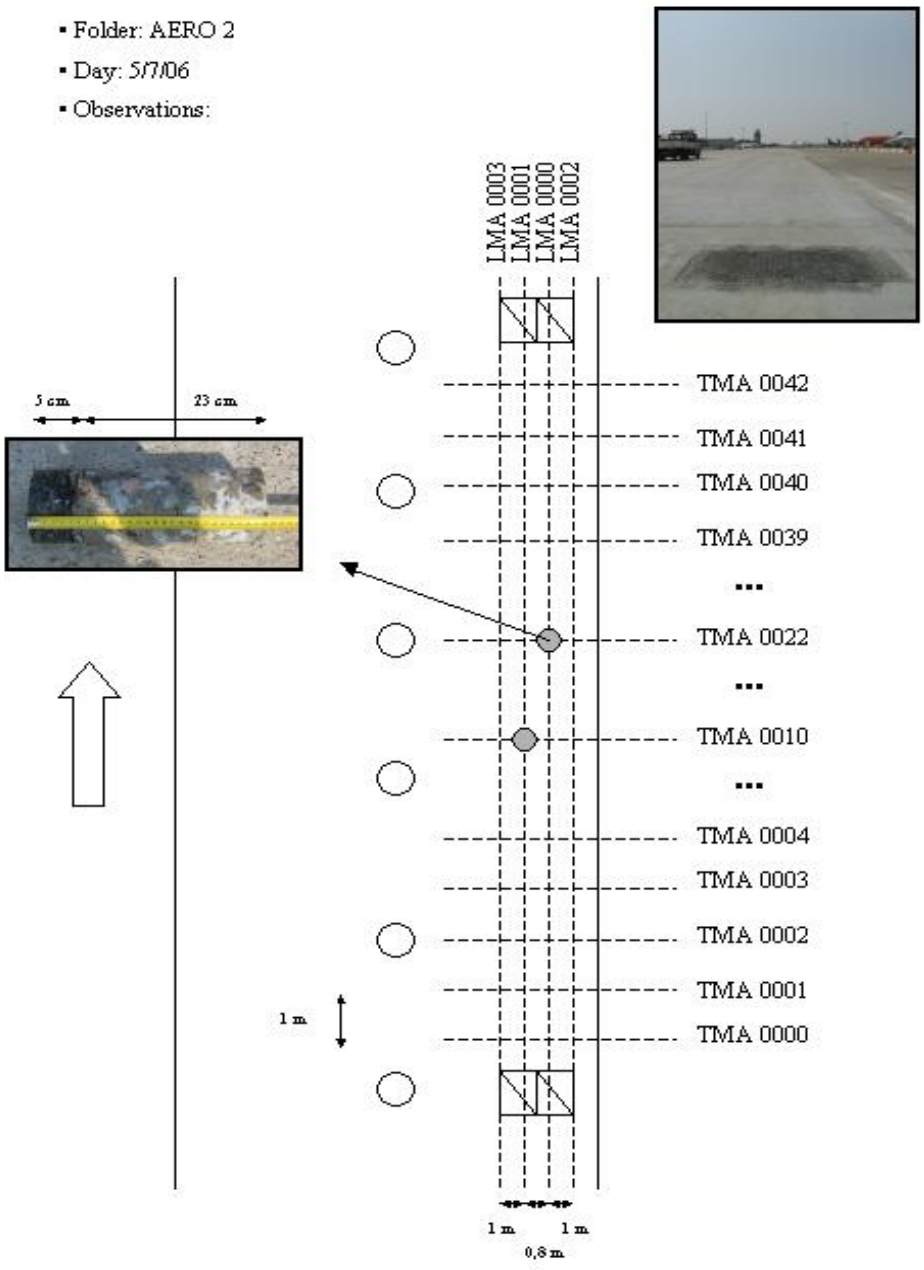

- Same scenario that the diagram before.
- 4 longitudinal scans over the energy supply wires (at the right side of the lights line – center-). 1m, 0.8m and 1m between scans.
- 43 transversal scans, at steps of 1m.
- Core samples of the ground at transversal scan

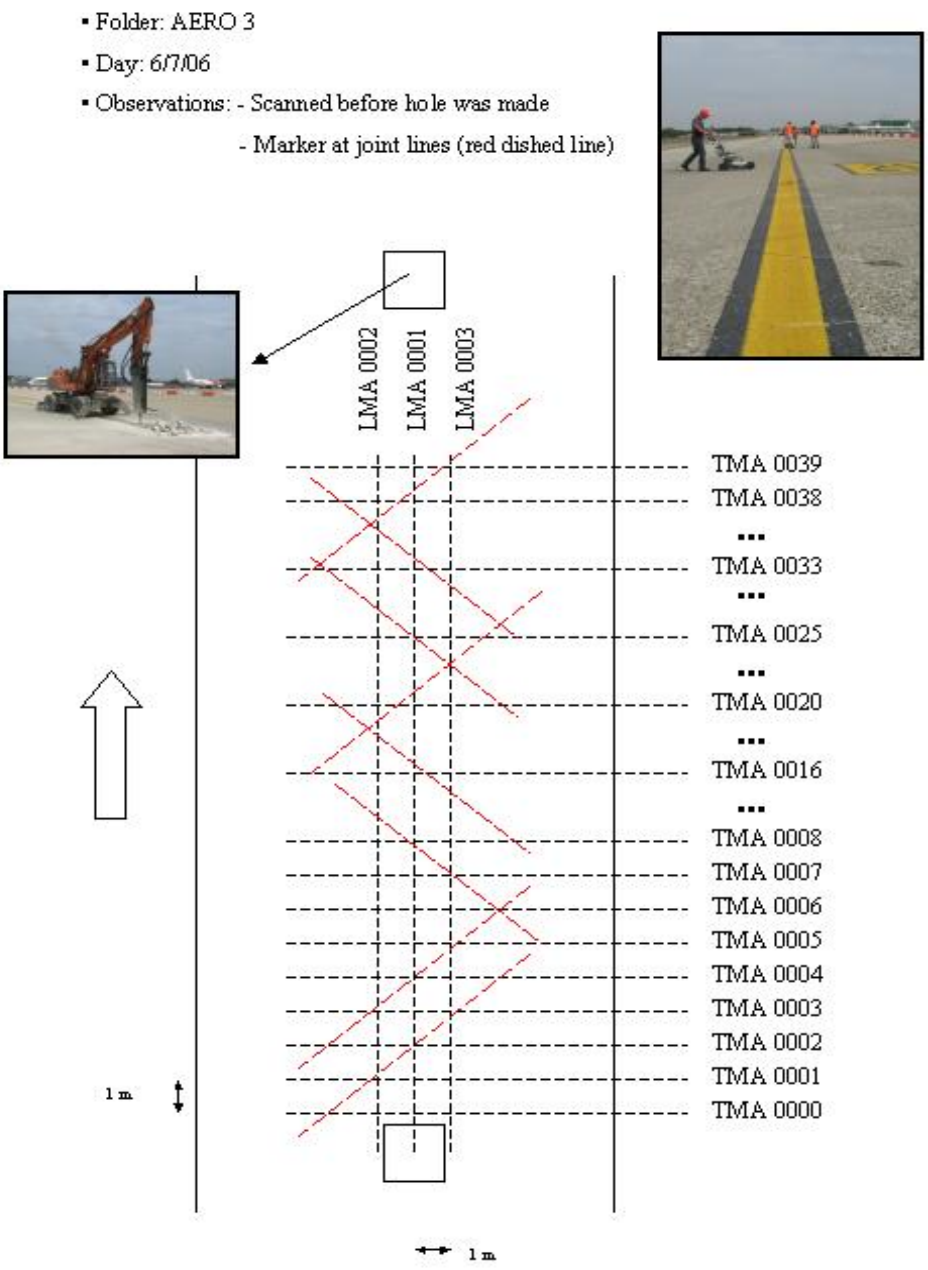

- Scan before the tunnel was made.
- 3 longitudinal scans. 1m distance between each one.
- 40 transversal scans at steps of 1m.
- Markers at pavement expansion joints (red dashed line).

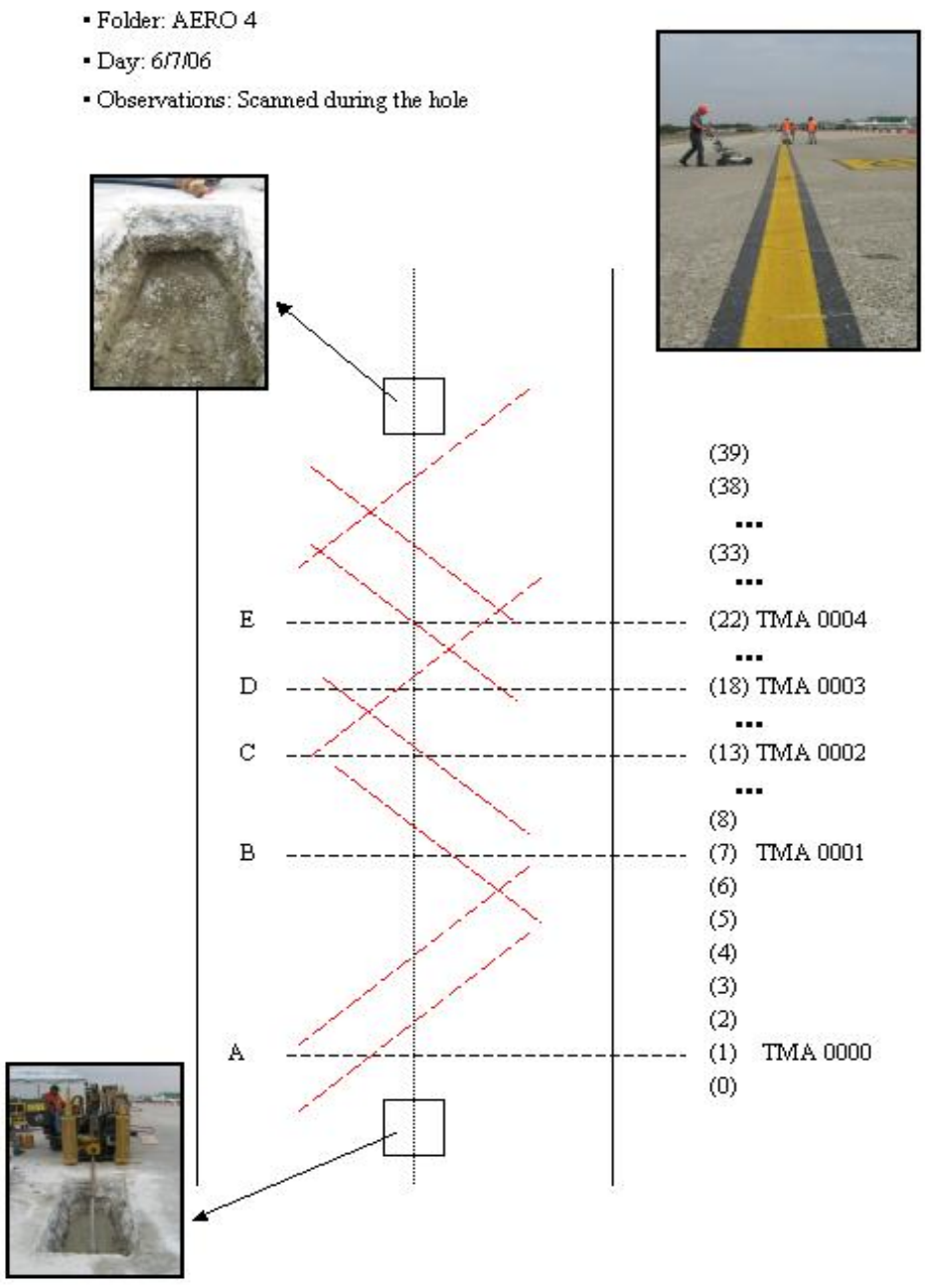

- Scan during the tunnel operation.
- 1 longitudinal scan.
- 40 transversal scans, 5 of them (A to E) of special interest due to 'particular' incidents that could be seen, as water emaining from the joints.

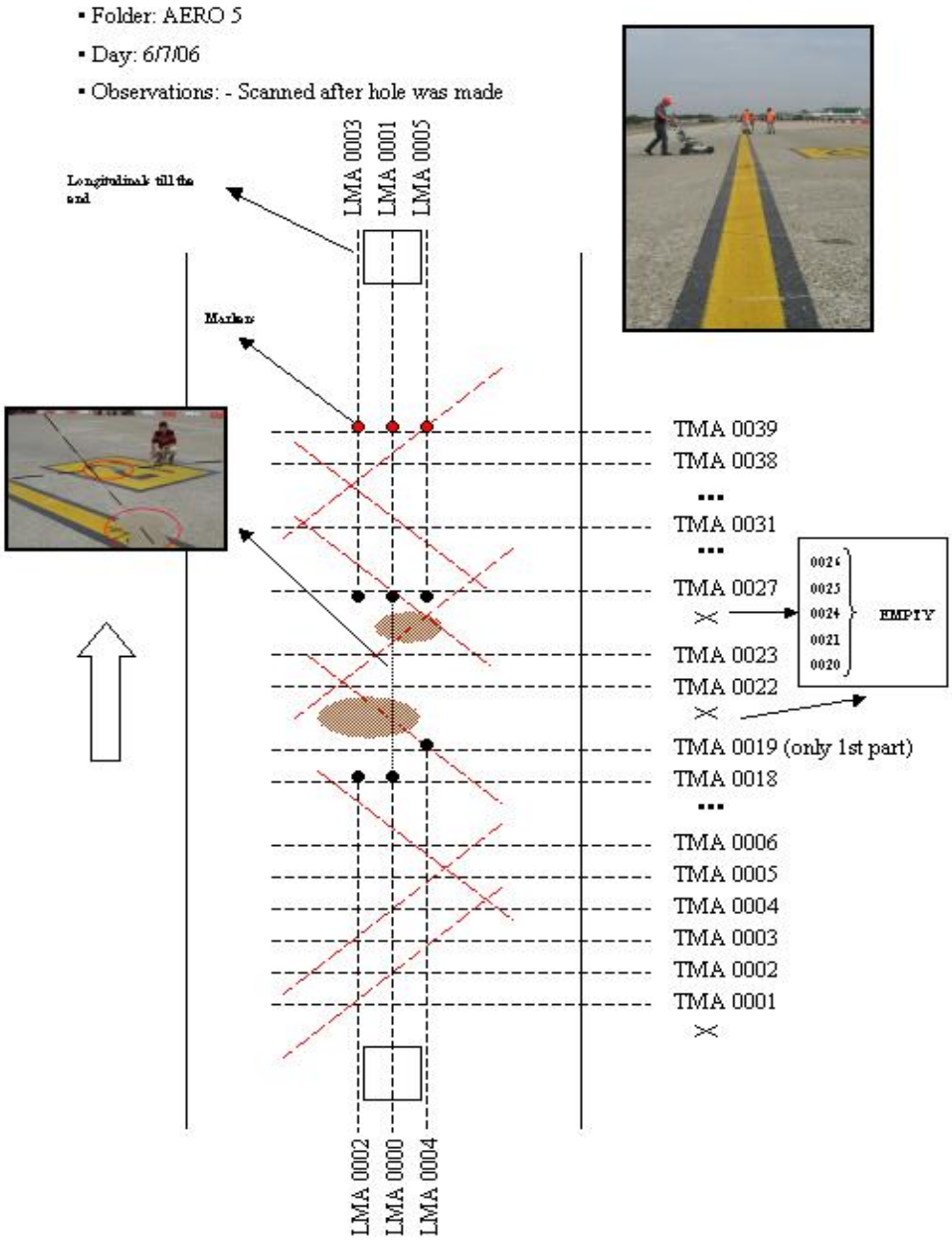

- Scan after hole was made.
- 3 longitudinal scans. Not complete scans as the middle part was full of mud from the inside the ground (emanated from the expansion joints)
- < 40 transversal scans (approx). We were unable to to the complete set of transversal scans as at parts there was mud on the ground.

APPENDIX B: The Matlab code

B.1. GRP calibration: the 'r' parameter estimation

```
function pushbutton1_Callback(hObject, eventdata, handles)
      % hObject    handle to pushbutton1 (see GCBO)
      % eventdata  reserved - to be defined in a future version of
MATLAB
      % handles    structure with handles and user data (see
GUIDATA)
      a1 = str2double(get(handles.a1, 'String'));
      if isnan(a1)
            set(hObject, 'String', 0);
            errordlg('Input must be a number','Error');
      end
      v2 = str2double(get(handles.v1, 'String'));
      if isnan(v2)
            set(hObject, 'String', 0);
            errordlg('Input must be a number','Error');
      end
      e1=1;
      v2=v2*1000000;
      e2=(3e8/v2)^2;
      r1=subs(solve('a1=r1*(e1^0.5-e2^0.5)/(e1^0.5+e2^0.5)'));
      set(handles.r1,'String',-r1);

      handles.e2=e2;
      guidata(hObject,handles);
      set(handles.pushbutton2, 'Enable','on');
```

B.2. GRP Echo detection and amplitude estimation

```
function [a_k,t_k,Sf]=echoes_detection(handles,s, A, A2,
numlayers, track_win_hook,   track_win_hold, iniaveragewin, w)
% s= respuesta impulsional del filtro ;
```

```
% A= mappa radar
% w=10;  distancia minima (en muestras) entre picos. dado por la
freq del radar...

set(handles.progress, 'visible', 'on');
v_avg=1e8;
tsweep=40e-9;
nsamples=512;

[m,n]=size(A);

a_k(numlayers,n)=0;
t_k(numlayers,n)=0;

Es=0;

for i=1:length(s)
    Es=(abs(s(i)))^2+Es;
end

for t=2:n
    prog=round((t/n)*100);
    prog2=num2str(prog);
    prog3=strcat(prog2,' %');
    set(handles.progress,'String',prog3);

    sf=filter(s/Es,-1,A(:,t));                  %MATCHED FILTER

    iniaveragewin5=4;               %averaging only for 1500
configuration
    if length(s)==17
        for d=125:length(sf)-iniaveragewin5
            sf(d)=sf(d)^3;                                      %make
peaks more significant
            sf(d)=mean((d/200)*abs(sf([d-
iniaveragewin5:d+iniaveragewin5]))); %lineal STC
```

```
        end
    else
        for i=1:length(sf)                % only positive
            if sf(i)<0
                sf(i)=sf(i)*0.1;
            end
        end
    end

    x=round(length(s)*1/2);
    for i=1:length(sf)-x
        sf2(i)=sf(i+x);
    end


    Sf(:,t)=sf2';

    sfm=sf2;                          %search in the (-) of the
absolut value of sf

    if t==2
        for g=1:track_win_hook
            sf3=filter(s/Es,-1,A(:,g));         %INITIALIZE
TRACKING

                                              %averaging only for 1500
configuration
            if length(s)==17
                for e=125:length(sf3)-iniaveragewin5
                    %c=e
                    sf3(d)=sf3(d)^3;
                    sf3(d)=mean((d/200)*abs(sf3([d-
iniaveragewin5:d+iniaveragewin5])));

                end
            else
                for i=1:length(sf3)       % only positive
```

```
                    if sf3(i)<0
                        sf3(i)=sf3(i)*0.1;
                    end
                end
            end

            y=round(length(s)*1/2);
            for p=1:length(sf3)-y
                sf4(p)=sf3(p+y);
            end

            sfM=sf4;
            for h=1:numlayers
                [valormax3,posmax3]=max(sfM);
                if controla(posmax3,sfM)==1
                    t_k(h,g)=posmax3;
                    for k=posmax3-w:posmax3+w
                        sfM(k)=0;
                end
            end

        end
        aux3=sort(round(mean(t_k(:,[1:track_win_hook]),2)));
        t_k(:,1)=aux3;
    end
    end

    for j=1:numlayers               %SEARCH FOR MAX'S
(iinterfaces)
        a=t_k(j,t-1)-track_win_hold ;
        b=t_k(j,t-1)+track_win_hold;
        %t
        aux=sfm( a : b  );
        [valormax,posmax2]=max(aux);
        posmax=posmax2+a-1;
            for k=posmax-w:posmax+w
                        sfm(k)=0;
```

```
            end
        a_k(j,t)=A2(posmax,t);
        if length(s)==17
            a_k(j,t)=Sf(posmax,t);
        end
        t_k(j,t)=posmax;
    end

    for j=1:numlayers-1                    ORDER FOR INCREASING
t_k's
        for k=j+1:numlayers
            if t_k(j,t)>=t_k(k,t)
                aux=t_k(k,t);
                t_k(k,t)=t_k(j,t);
                t_k(j,t)=aux;
                aux=a_k(k,t);
                a_k(k,t)=a_k(j,t);
                a_k(j,t)=aux;
            end
        end
    end
end

%w1=5;                          % AVERAGING
%smooth_win=15;
for d=iniaveragewin+1:n-iniaveragewin
    for u=1:numlayers
        t_k(u,d)=mean(t_k(u,[d-iniaveragewin:d+iniaveragewin]));
        a_k(u,d)=mean(a_k(u,[d-iniaveragewin:d+iniaveragewin]));

      end
  end

  w2=round(n*0.01);                %PICK ONLY CENTRAL PART OF THE
MATRIX
  a_k=a_k(:,[1+w2:n-w2]);
  t_k=t_k(:,[1+w2:n-w2]);
```

```
a_k=-a_k
t_k
set(handles.progress, 'visible', 'off');
```

B.3. GRP Layer-stripping algorithm

```
function [e,z]=layer_stripping(a, t,
handles,iniaveragewin,numlayers,eas)
t=t*40e-9/512;                              % 1 sample = 40ns / 512
samples/column
                                        % t=time of delay matrix

[numero_reflex, numero_sweeps]=size(a);        %amplitude of
reflexion matrix
numero_stratos=numero_reflex-1;

c=3e8;
z(numero_reflex,numero_sweeps)=0;
z(1,:)=(1e-8)*t(1,:)/2;
e(numero_reflex,numero_sweeps)=0;
e(1,:)=1;

set(handles.progress, 'visible', 'on');

r=eas';                                 % equivalent atenuation set
(depends on the application)
if handles.data11 == 1
    eqatset=handles.data10;
    r=eqatset';
end

tau=1;
for j=1:numero_sweeps
    for i=1:numero_stratos
        A=a(i,j); E=e(i,j); Z=z(i,j);
t2=t(i+1,j);t1=t(i,j);R=r(i);
```

```
        if i<2
            e2=subs(solve('A=R*(E^0.5-e2^0.5)/(E^0.5+e2^0.5)'));
        else
            tau=tau*4*(e(i-1,j)^0.5*e(i,j)^0.5)/
(e(i-1,j)^0.5+e(i,j)^0.5)^2;
            T=tau;
            e2=subs(solve('A=R*((E^0.5-e2^0.5)/
(E^0.5+e2^0.5))*T'));
            tau=1;
        end

            z2=Z+(e2^(-0.5))*( t2-t1 )*(c/2);
        e(i+1,j)=e2;
        z(i+1,j)=z2;

        prog=round((j/numero_sweeps)*100);
        prog
    prog2=num2str(prog);
    prog3=strcat(prog2,' %');
    set(handles.progress,'String',prog3);
end

end

z=z*100
e

iniaveragewin=iniaveragewin*2;
for d=iniaveragewin+1:numero_sweeps-iniaveragewin
    for u=1:numlayers
        z(u,d)=mean(z(u,[d-iniaveragewin:d+iniaveragewin]));
        e(u,d)=mean(e(u,[d-iniaveragewin:d+iniaveragewin]));
    end
end
```

B.4. GRP Layer thickness and permittivity plot

```
z_k=handles.data3;
e_k=handles.data4;

[numero_reflex,numero_sweeps]=size(z_k);
axes(handles.axes4);

e_max=max(max(e_k))
e_min=min(min(e_k(2:numero_reflex,:)))

for j=1:numero_sweeps
    for i=1:numero_reflex-1
        if numero_sweeps < 100
             line([j j],[z_k(i+1,j) z_k(i,j)],'color',[1   1-
e_k(i+1,j)/e_max    1-e_k(i+1,j)/e_max],'linewidth',4.5);
        elseif numero_sweeps < 150
             line([j j],[z_k(i+1,j) z_k(i,j)],'color',[1   1-
e_k(i+1,j)/e_max    1-e_k(i+1,j)/e_max],'linewidth',3);
        elseif numero_sweeps < 200
            line([j j],[z_k(i+1,j) z_k(i,j)],'color',[1    1-
e_k(i+1,j)/e_max    1-e_k(i+1,j)/e_max],'linewidth',2.5);
        elseif numero_sweeps < 900
            line([j j],[z_k(i+1,j) z_k(i,j)],'color',[1    1-
e_k(i+1,j)/e_max    1-e_k(i+1,j)/e_max],'linewidth',1.5);
        else
             line([j j],[z_k(i+1,j) z_k(i,j)],'color',[1   1-
e_k(i+1,j)/e_max    1-e_k(i+1,j)/e_max],'linewidth',1);
        end
        grid on;
        axis ij;
    end
end
axis auto;
grid on;
axis ij;
set(handles.axes4,'ytickmode','auto');
```

```
get(handles.axes4)
xlabel('sweep');
ylabel('depth (cm)');


set(handles.colormax,'backgroundcolor',[1 0 0]);
set(handles.colormin,'backgroundcolor',[1 1-e_min/e_max 1-
e_min/e_max]);
set(handles.emax,'string',num2str(round(e_max)));
set(handles.emin,'string',num2str(round(e_min)));

axes(handles.axes5);
for i=1:numero_reflex
    e_mean=mean(e_k(i,:));
    z_max=max(z_k(i,:));
    z_min=min(z_k(i,:));
    if i==1
        line([e_mean e_mean],[0 z_min],'linewidth',2);
    else
        line([e_mean e_mean],[max(z_k(i-1,:))
z_min],'linewidth',2);
    end
    if i<numero_reflex
        line([e_mean mean(e_k(i+1,:))],[z_min
z_max],'linewidth',2);
    end
end

axis auto;
axis ij;
grid on;

try
var=get(handles.axes4,'ytick');%%%
var2=get(handles.axes4,'ylim');
```

```
%set(handles.axes5,'xtick',
[round(mean(e_k,2))],'ytick',var,'ylim',var2,'YAxisLocation','left
');
xlabel('permittivity');

catch
     errordlg('An error ocurred during the plot. The graph could
be not well done','PLOT ERROR');
 end
```

APPENDIX C: GPROMA3 Application help file

To launch the application just type 'gproma3' at the console view of Matlab (gproma3.m and gproma3.fig must be in the work directory).
Select an input file (data matrix out of the radar).

Some notes about most common parameters values...

- **Number of Layers:** "3" for 600 MHz - 600 MHz (air/usura+binder/base)
  "4" for 1500 MHz - 1500 MHz (air/usura/binder/base)

- **Hook Tracking Window:** Number of samples that are used to calculate the initial interfaces position. The algorithm takes the firsts "hook tracking window" samples of the time-delay matrix and do the average with them. those initial values are used to know where the interfaces start and to initiate the tracking algorithm. usually is enough with 10 or 20 samples.

- **Hook Tracking Window:** Maximum allowed difference in samples between a single echo detection and its following one. Hook Tracking Window should be selected as a compromise between low tracking noise (small value) and good tracking capability of rapid interface variations (large value). Usually 10 samples is an appropriate value.

- **Smoothness Window:** A Low-Pass Filter is applied at the echo-delay matrix in order to clear and smooth the result of false detections, due to possible errors in the tracking phase. Larger value means smooth detection but possible missing of rapid variations in the interfaces. Smaller value means abrupt interfaces but possible false detections in some points.
  Recommended: "10" for 600 - 600 MHz; "20" for 1500 - 1500 MHz.

- **Post-Averaging:** Same as Smoothness Window but for apply after the echo-detection. Just in cases the result was too abrupt.

- **Cut Sides:** Many times the echo-detection is wrong at first samples (or last) as there is a "transition period" in which the algorithm is not stable. In order to avoid further errors at

the Layer-Stripping algorithm it is recommend to clear those samples entering the number of "wrong" samples en then push "Redraw".

- **Equivalent Attenuation Set (EAS):** The algorithm is calibrated for work with most common asphalt values. Whenever you want to study another kind of surfaces you have to enter new values for the EAS.

Procedure:

1- Enter algorithm parameters and then push "Echoes Detection"

2- Execute "eas" in the Matlab command window. The assistant for calculate the new EAS will open.

3- Now you have to enter velocity of propagation (VOP) and reflexion amplitude (RA) of every layer.

4- Calculate VOP with the help of the "Average values" given in the "Echoes detection".

Note that:

1 sample = 40ns/512

v=e/t=(2*z)/t

"t" is the time used by the signal to go and back through a single layer.

"z" is the value for the depth of the layer, so a sample core is needed for the calibration

5- Introduce VOP's and RA's. For example, in the first line you have to enter the RA of the "air-ground" interface and the VOP of the first layer of the ground (air doesn't count).

6- Once you have the new EAS you can introduce it by entering the values in the cells and pushing "Intro array". Then push "Layer-Stripping" as usual.

BIBLIOGRAPHY

[1] ”Reliability of signal processing technique for pavement damages detection and classification using ground penetrating radar”. *Andrea Benedetto, Francesco Benedetto, Maria Rosaria De Blasiis and Gaetano Giunta*

[2] “Localized Parametric electromagnetic inversion for pavement profiling with ground penetrating radar”. *Weikun He, Jiaxue Liu and Renbiao Wu*

[3] “An efficient Algorithm for time delay estimation”. *Li, Jian and Renbiao Wu*

[4] “Permittivity measurements of multilayered media with monostatic pulse radar”. *Umberto Spagnolini*

[5] “Multitarget detection/tracking for monostatic ground penetrating radar: application to pavement profiling”. *Umberto Spagnolini and Vitorio Rampa*

[6] “Ground penetrating radar tomography”. *John E. Molyneux*

[7] “Modeling of Ground-Penetrating Radar for Accurate Characterization of Subsurface Electric Properties”. *Sébastien Lambot, Evert C. Slob, Idesbald van den Bosch, Benoit Stockbroeckx, and Marnik Vanclooster*

[8] “GPR for Archaeological Investigations: Real Performance Assessment for different Surface and Subsurface conditions”. *Massimo Sciotti, Fabiola Colone, Debora Pastina, Tullio Bucciarelli*

[9] “Applications of GPR for surface mining”. *Jan C. Francké*

[10] “Computing system processing of GPR sounding profiles”. *M. Dascilu, E. D. Franti'*

[11] “Continuous pavement profiling with ground-penetrating radar”. *R. Wu. X. Li and J. Li*

[12] “Diagnosis of pavement structural damages using GPR”. *A. Benedetto, S. Pensa*

[13] “GPR-History, Trends, and Future Developments”. *A. P. Annan*

[14] “Interface identification using a GPR signal: A Monte Carlo Markov Chain approach”. *Arnaud Coatanhay, Jean-Jacques Szkolnik.*

[15] “GPR migration algorithm for landmines buried in inhomogeneous soil”. *M. Sato and X. Feng*

[16] “Measuring Soil Water Content with Ground Penetrating Radar: A Review”. *J. A. Huisman,* S. S. Hubbard, J. D. Redman, and A. P. Annan*

[17] “Realistic modeling of surface ground-penetrating radar antenna system: where do we stand?”. *K. Holliger, B. Lampe**,** U. Meier, M. Lambert, A.G. Green*

[18] “Regularization of Laplace transform inversion for subsurface conductivity and permitivity profile estimation using GPR signals.”. *A. Coatanhay*

[19] “Simulations of Ground-Penetrating Radars Over Lossy and Heterogeneous Grounds”. *Levent Gürel*

[20] “Subssurface permittivity permittivity estimation from ground-penetrating radar measurements”. *Paul D. Walker*

[21] “Application of Texture Feature Classification Methods to Landmine/Clutter Discrimination in Off-Lane GPR Data”. *Peter Torrione, Leslie Collins*

[22] “Velocity variations and water content estimated from multi-offset, ground-penetrating radar”. *Robert J. Greaves*, David P. Lesmes*, Jung MO Lee*, and M. Nafi Toksöz**

[23] “Model based signal processing for MIDP radar” (.ppt) *Information and Telecommunication Center. University of Kansas*

[24] “Adaptive B-spline scheme for solving an inverse scattering problem*” Alexandre Baussard, Eric L Miller and Denis Premel*

[25] “FPGA based architecture for radar's STC, FTC and gain modules” *Joaquín Garcia, Gilberto Viveros, René Cumplido*